UNIVERSITY OF AGDER

# Electromechanical characterization of superconducting wires and tapes at 77 K

Keywords: high temperature superconductor, strain dependent critical current measurement, tensile test, x-ray diffraction

*Author:*
**Roger Bjoerstad**

*Supervisor at CERN:*
Christian Scheuerlein M.Sc.

*Supervisor at*
*University of Agder:*
Prof. Tor Oskar Saetre



*This Bachelor's Thesis is carried out as a part of the education at the University of Agder and is therefore approved as a part of this education. However, this does not imply that the University answers for the methods that are used or the conclusions that are drawn.*

University of Agder, February 27, 2015
Faculty of Engineering and Science
Department of Engineering

# Abstract

The strain dependency of the critical current ($I_c(\varepsilon)$) in state-of-the-art cuprate high-temperature superconductors (HTS) has been characterized. A universal test machine (UTM) combined with a critical current measurement system has been used to characterize the mechanical and the $I_c(\varepsilon)$ properties of conductors immersed in an open liquid nitrogen dewar. A set-up has been developed in order to perform simultaneous measurements of the superconductor lattice parameter changes, critical current, as well as the stress and strain at 77 K in self-field in a high energy synchrotron beamline.

The HTS tapes and wires studied were based on YBCO, Bi-2223 and Bi-2212. The YBCO tapes were produced by SuperPower and American Superconductors (AMSC). Two types of Bi-2223 tapes, HT and G, were produced by Sumitomo Electric Industries (SEI). The Bi-2212 wires were produced by Oxford Superconducting Technology (OST) using Nexans granulate precursor, before undergoing a specialized over pressure (OP) processing and heat treatment to optimize $I_c$ at 77.

The mechanical properties were determined from engineering stress-strain ($\sigma(\varepsilon)$) curves, and $I_c(\varepsilon)$ characteristics were established at 77 K in self-field. The irreversible strain limit, $\varepsilon_{irr-5\%}$, defined as a 5% permanent reduction in $I_c$, was observed in the YBCO tapes at 1.05% by AMSC, and 0.72% by SuperPower. For the Bi-2223 samples, the $\varepsilon_{irr-5\%}$ was determined to be at the fracture strain, 0.4% for Type HT and 0.2% for Type G. The Bi-2212 wire showed an $\varepsilon_{irr-5\%}$ at 0.6% strain.

The combined lattice parameter, critical current, stress and strain measurements of the Bi-2212 wire and Bi-2223 tape in the high energy synchrotron beamline show that the superconducting portion deforms elastically until the irreversible strain limit is reached.

# Acknowledgments

All experiments described in this thesis were funded by CERN.

I would like to express my sincere gratitude to my CERN supervisor, Christian Scheuerlein M.Sc, for giving me the possibility to partake in this interesting experiment and the valuable assistance he has given me while writing this thesis.

Special thanks to academic supervisor at University of Agder Professor Tor Oskar Saetre.

Thanks to Jerôme Fleiter, Ph.D, for instructions on critical current measurement and analysis of resulting data.

I would like to give a special thanks to Michinaka Sugano, Ph.D, of the KEK University for valuable advice regarding strain dependent critical current measurement on high-temperature superconductors.

Thanks to beam scientist Jessica Hudspeth, Ph.D at ESRF, for assistance and instructions during experiments at the ID15B beamline.

Special thanks to Dr. Mark Rikel from Nexans for collaboration during peak identifications and analysis for diffraction patterns.

Thanks to Julien Hurte, Philippe Denis, Marina García González, Alain Gharib, Andre Jacquemod, Jonathan Davoust, Bouchta Tbatou, Alejandro Sanz Ull and Jean-Sebastien Denis for technical assistance and sample preparation.

# Contents

# List of Figures

# List of Tables

# 1 Introduction

The European Organization for Nuclear Research (CERN) near Geneva in Switzerland is an international scientific institution dedicated to the study of high-energy particle physics. Scientists and engineers from around the world collaborate to conduct experiments and research.

With a circumference of 27 km the Large Hadron Collider (LHC) is the largest scientific instrument ever constructed. Consisting mainly of 1232 main dipole bending magnets and 392 quadrupole focusing magnets, the twin beamed collider is designed to accelerate protons to energy levels of 7 TeV per beam, resulting in a center-of-mass collision energy of 14 TeV. Four separate detectors; ATLAS, CMS, Alice and LHC-b is used to study the decay products of collisions [2].

In order to produce collisions of such energies, superconducting (SC) magnets are used to guide and to focus the particle bunches. The beam energy of a proton accelerator scales with the magnetic field of the bending magnets. The niobium-titanium (NbTi) superconducting main magnets of the LHC produces a peak magnetic field of 8.3 T when cooled down to 1.9 K, using superfluid helium [3]. Figure 1 shows a cross-sectional view of the superconducting dipole magnet of the LHC.

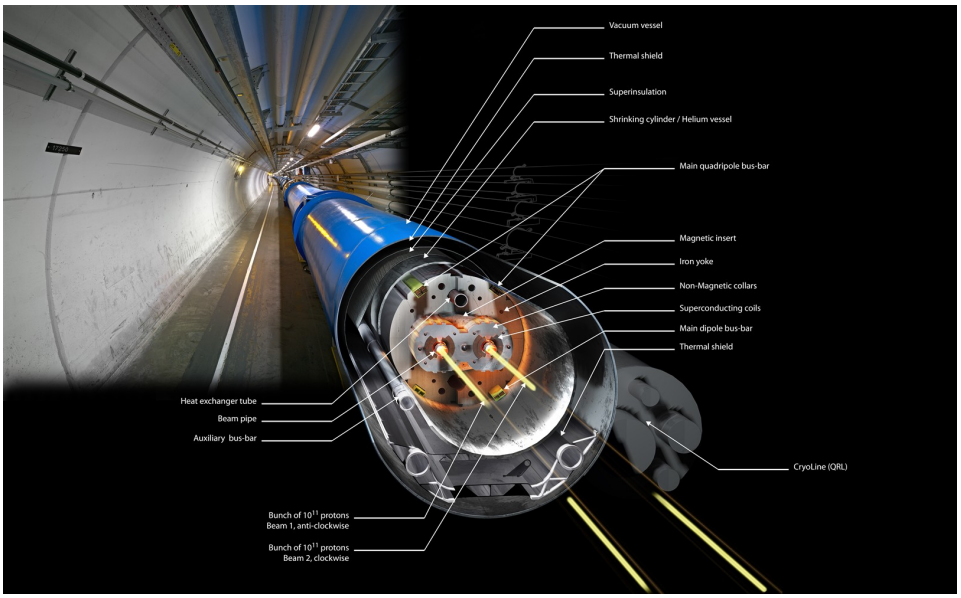


**Figure 1: Cross-sectional view of a superconducting dipole magnet of the LHC used to guide the particles during operation [1].**

Cuprate superconductors, such as Y-Ba-Cu-O (YBCO) and Bi-Sr-Ca-Cu-O (BSCCO), that have critical temperatures above 77 K are known as high-

temperature superconductors (HTS). Such HTS produces very high fields when cooled down with liquid helium, which will be required when building future 20 T accelerator magnets [4][5].

A drawback of cuprate superconductors is that they are brittle and exhibit a reduction of $I_c$ when subjected to straining [6][7]. Initially, the strain dependency of the critical current ($I_c(\varepsilon)$) is reversible, meaning that when the load is removed from the conductor the $I_c$ returns to the original value. However, when the irreversible strain limit ($\varepsilon_{irr-5\%}$) is exceeded the $I_c$ drops rapidly and the conductor's performance is permanently reduced.

Strain may be the result of manufacturing, coil winding or thermal contractions. Additionally, a conductor is subjected to a force known as the *Lorentz' force* when exposed to a magnetic field. It is therefore imperative to understand the strain dependent degradation of the HTS before large-scale practical implementation.

A set-up that can be used to study the strain dependency of the critical current of HTS is required, and the development of this system is the main subject of this thesis. Further, the system will be used to perform measurement of the electromechanical properties and the strain limit at which an irreversible degradation occurs in different HTS. The system will consist of a universal test machine (UTM) and extensometer combined with a critical current measurement system that can be used to characterize the electromechanical properties of HTS immersed in liquid nitrogen at 77 K in a open dewar.

Finally, in order to better understand the failure mechanisms of the internal structure of the superconductors, the set-up will be integrated into a high energy synchrotron beamline which will for the first time make it possible to measure the relative d-spacing changes simultaneously with the superconductor critical current, stress and strain.

# 2 Theory

This section describes fundamental concepts regarding mechanical properties of materials, superconductivity and superconducting materials, strain dependency of critical current and x-ray diffraction.

## 2.1 Mechanical properties of materials

When subjected to an increasing load, a material displays elastic and plastic deformation. In the elastic region the sample will return to its original length when the load is released, while a plastic deformation permanently alters the elongation of the sample.

The mechanical properties of the sample materials are determined by plotting engineering stress as a function of strain ($\sigma(\varepsilon)$), where engineering stress ($\sigma$) is defined as the applied force normalized to the original unloaded cross sectional area ($A_0$) of the sample, and the strain ($\varepsilon$) is the percentage elongation of the sample. From the $\sigma(\varepsilon)$ curves the moduli of elasticity, offset yield strength and the maximum stress and strain will be determined. Figure 2 shows a graphical representation of the mechanical properties.

**Modulus of elasticity**
The modulus of elasticity describes how a material deforms when subjected to a mechanical load [8, p.334]. Wire samples and tapes with a low cross-sectional area are often bended, which results in irreproducible initial portions of the $\sigma(\varepsilon)$ curves as they straighten out during loading. Due to this, the modulus of elasticity is determined by an unloading line ($E_a$), produced by unloading the sample in the elastic portion of the $\sigma(\varepsilon)$ curve.

**Offset yield strength and strain**
Some ductile materials show little to no evidence of a clear yield point. As a result of this, the offset yield strength ($R_{p0.2}$) and strain ($\varepsilon_{p0.2}$) is used as a substitute of the yield point. The $R_{p0.2}$ is defined as the stress which produces a 0.2% plastic deformation [8, p.332], while the $\varepsilon_{p0.2}$ is the corresponding strain at $R_{p0.2}$. $R_{p0.2}$ is determined as the intersection between the $\sigma(\varepsilon)$ curve and a line that starts in $\varepsilon = 0.2\%$ with the slope equal to the $E_a$ of the sample.

**Maximum stress and strain**
The maximum stress ($R_{max}$) and strain ($\varepsilon_{max}$) is defined as the engineering stress and strain recorded at the event of sample fracture during a tensile test. If the tensile loading is ceased before a fracture occurs, $R_{max}$ and $\varepsilon_{max}$ is reported to be greater than the highest measured value of stress and strain, respectively.

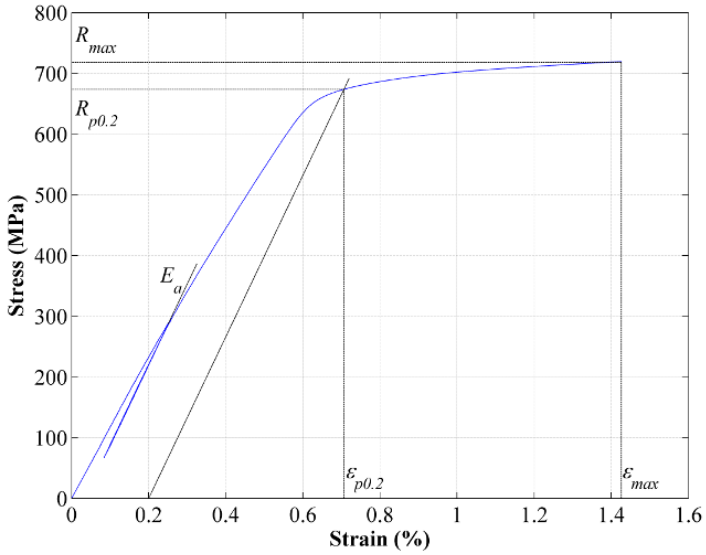


**Figure 2: Engineering stress-strain curve of a SuperPower YBCO tape with definition of the modulus of elasticity under decreasing ($E_a$) load, offset yield strength ($R_{p0.2}$) and strain ($\varepsilon_{p0.2}$), and maximum stress ($R_{max}$) and strain ($\varepsilon_{max}$).**

## 2.2 Superconductivity

A superconductor is a material which conducts, under the right conditions, an electric current with practically zero resistance. In order to achieve superconductivity the conductor must be cooled down below its critical temperature ($T_c$). The upper limit of current that can be transported through the conductor is the critical current ($I_c$), while the upper limit of magnetic field that the conductor can be subjected to is the critical field ($H_c$) [9, p. 864]. Figure 3 shows a three dimensional graphical representation of the $I_c$ as a function of temperature ($T$) and magnetic field ($H$) of a non-specific superconductor. The resulting critical surface is the volume where the conductor is superconducting. Practical applications for superconductors include high-energy physics, magnetic resonance imaging and power transmission lines.

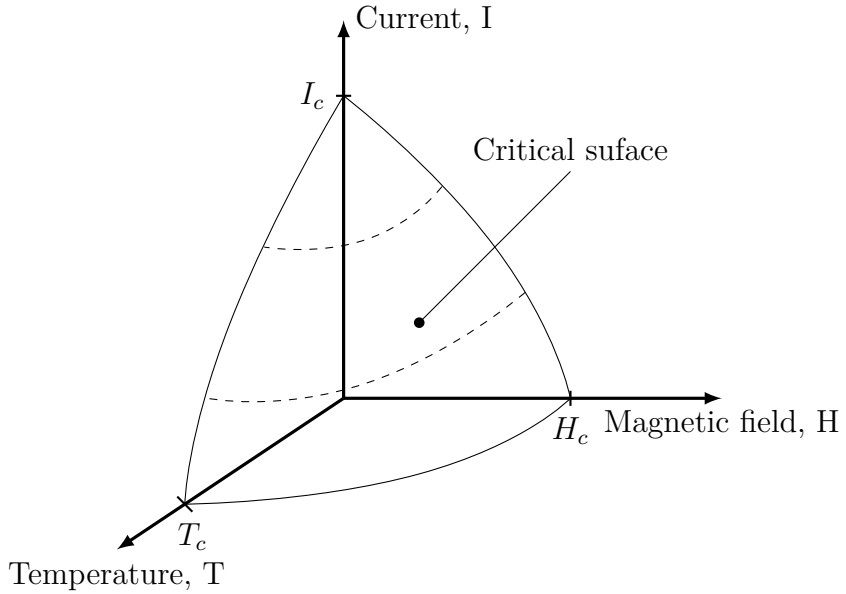


**Figure 3: Critical surface of a non-specific superconductor. The temperature, magnetic field and current density must be below the critical surface to achieve a superconducting state.**

### High-temperature superconductors

A number of ceramic copper-oxide (cuprate) conductors exhibits superconductivity at temperatures above 77 K. These conductors are referred to as high-temperature superconductors (HTS). The high $T_c$ means that liquid nitrogen ($LN_2$), which boils at 77.4 K at 1 atmosphere [10, p. 9], can be used as a refrigerant instead of helium. This study focuses on the electromechanical properties of YBCO, Bi-2223 and Bi-2212 superconductors in $LN_2$ .

### Strain dependency of the critical current

The critical current in composite superconductors degrade when the conductor is subjected to compressive and tensile strain[10, p. 432]. In practical examples such strains may be the result of:

- **Manufacturing:** Winding spools and coils of wires and tapes.
- **Thermal contraction:** A composite might have constituents with differing thermal contraction coefficients producing internal strains. Soldering two materials with different thermal contraction coefficients may produce unwanted straining on the superconducting material.
- **Lorentz force:** When a conductor, which is transporting a current, is subjected to a magnetic field a load known as *Lorentz force* is generated which is proportional to said current and field [11, p. 27].

Figure 4 shows the relative $I_c$ degradation ($I_c/I_{c0}$) as a function of strain. A sample is strained to a certain elongation, and the $I_c$ is measured, illustrated by the 'x'. When the load is released and $I_c$ is re-measured, illustrated by the 'o', the $I_c$ returns to a value at the corresponding sample elongation. As long as the returned $I_c$ falls on the previous value, the $I_c$ is regarded as *reversible*. $\varepsilon_{95\%}$ is defined as the strain where a reversible 95% retention in $I_c$ is observed.

When the returned value of $I_c$ falls lower than the initial measured $I_c$, the superconductive portion of the sample is damaged and the reversible strain effect dissipates. This transition is called the *irreversible strain limit*, or $\varepsilon_{irr-5\%}$. As seen in Figure 4, the load is periodically returned from the non-primed to the corresponding primed letter where $I_c$ is re-measured. As long as $\varepsilon_{irr-5\%}$ is not reached, the $I_c$ should be the same upon returned, as mentioned above. $\varepsilon_{irr-5\%}$ is defined as the strain which produces a permanent $I_c$ reduction, and in this study the definition of $\varepsilon_{irr-5\%}$ is the strain which produces a 5% permanent reduction in $I_c$ upon returning. While A' falls very close to the initial $I_c$ and B' is showing a hint degradation, $\varepsilon_{irr-5\%}$ is not reached until the sample is strained to C where C' shows a 5% reduction.

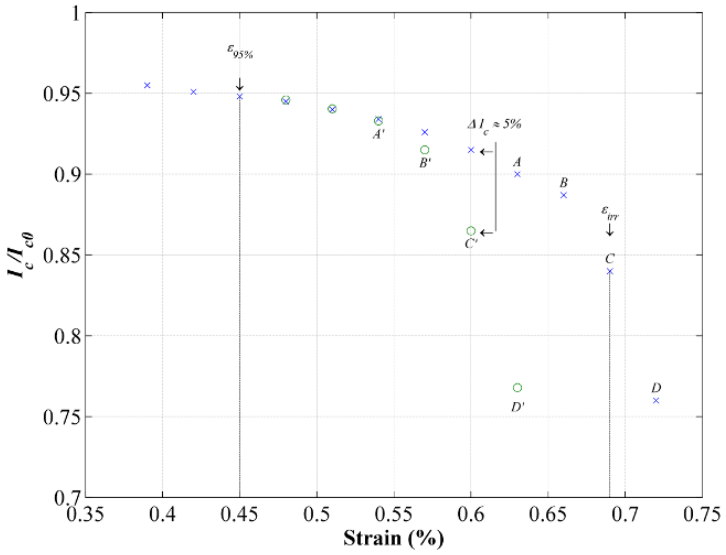


**Figure 4: Strain dependent degradation of $I_c$ under axial straining and definition of 95% retention of $I_c$ and the irreversible strain limit. The load is returned from the non-primed letters at $I_c$ is remeasured to determine is there has been a permanent degradation of the sample.**

## 2.3 X-ray diffraction

X-ray diffraction (XRD) is a non-destructive method of measuring lattice parameters in crystalline structures. By exposing a crystalline solid to x-rays, the resulting diffracted beam can be used to measure the distance between the lattice planes, known as the *d-spacing* ($d_{hkl}$) [9, p.117]. The relationship between the $d_{hkl}$ and incident x-ray is given by *Bragg's law* described in Equation 1 [12]

$$n\lambda = 2d_{hkl}\sin\theta \tag{1}$$

*Where:*

| | |
|---|---|
| $d_{hkl}$ | is the *d-spacing* (Å) |
| $\lambda$ | is the photon wavelength of the beam (Å) |
| $\theta$ | is the angle between incident ray and scattering plane |
| $n$ | is the order of diffraction |

# 3 Experimental

This section will start by identifying potential hazards of experiments at cryogenic temperatures. Then an introduction of the samples is given and the necessary sample preparation is described. Following this is the details of the experimental hardware and procedures for tensile tests and critical current measurements. Lastly, the set-up prepared for combined stress-strain, $I_c$, and lattice distortion measurements at the ESRF ID15B beamline is described.

## 3.1 Health and safety

**Cryogenic hazard**
Liquid nitrogen exposed to open air is used as the coolant during characterization of the electromechanical properties of the HTS samples. $LN_2$ has a boiling point of 77 K at 1 atm ($-196\,^{\circ}C$). Direct contact may cause cold burns to skin, or damage to vision. Metallic objects that have recently been immersed in $LN_2$ may fuse to skin upon contact. Cryogenic grade gloves must be used when handling $LN_2$ and recently cooled objects. Goggles or visor must be worn at all times. Additionally, personnel must have sufficient safety training to transfer $LN_2$ containing vessels.

When $LN_2$ transits from liquid to gas state it does so with a volumetric ratio of 1:694 [13]. The vaporized nitrogen will displace oxygen in the surrounding atmosphere, and spillage in close confinements can cause asphyxiation dangers.

**Electric shock hazard**
The Power supply used in critical current measurement uses low voltage and high currents which may produce arcs and burns if short circuited. Necessary steps shall be taken to isolate cables and leads.

## 3.2 The Samples

The samples studied are monofilament YBCO second-generation (2G) HTS tapes produced by American Superconductors (AMSC) and SuperPower, multifilament Bi-2223 tapes produced by Sumitomo Electric Industries, LTD (SEI) and multifilament Bi-2212 wires by Oxford Superconducting Technology (OST). An overview of the sample is given in Table 1.

**Table 1: Summary of the samples studied, showing manufacturer, type, superconducting material, measured cross-sectional area (measured on at least three samples) and providers ID-number.**

| Manufacturer | Type | SC-material | Cross-section ($mm^2$) | ID-number |
|---|---|---|---|---|
| AMSC | Type 8700 | YBCO | $1.954 \pm 0.016$ | 556B-2-32-131 |
| SuperPower | SCS4050 | YBCO | $0.410 \pm 0.020$ | 20110701 |
| SEI | Type HT | Bi-2223 | $1.637 \pm 0.023$ | CETS 10-044-01 |
| SEI | Type G | Bi-2223 | $1.010 \pm 0.005$ | CETS 11-057-02 |
| OST | OP processed | Bi-2212 | $\varnothing 0.477 \pm 0.002$ | PMM130723-2 |

### YBCO Type 8700 from AMSC

The YBCO Type 8700 556B-2-32-131 produced by AMSC consists of a film of a 0.8 $\mu$m thick YBCO layer on a substrate of Ni-5%at.W. The YBCO and substrate is sandwiched between two layers of brass to provide stabilization and reinforcement [14].

### YBCO SCS4050 from Superpower

The YBCO SCS4050 20110701 tape produced by SuperPower consists of a 1 $\mu$m thick YBCO layer, deposited on a stack of textured buffer layers. The buffer layers are deposited on a 50 $\mu$m thick Hastelloy C-276 substrate. The YBCO and substrate are sandwiched between two 2 $\mu$m thick Ag layers and surrounded by a 20 $\mu$m thick copper stabilizing layer. Figure 5 shows a schematic view of the structure of the YBCO tape by SuperPower.

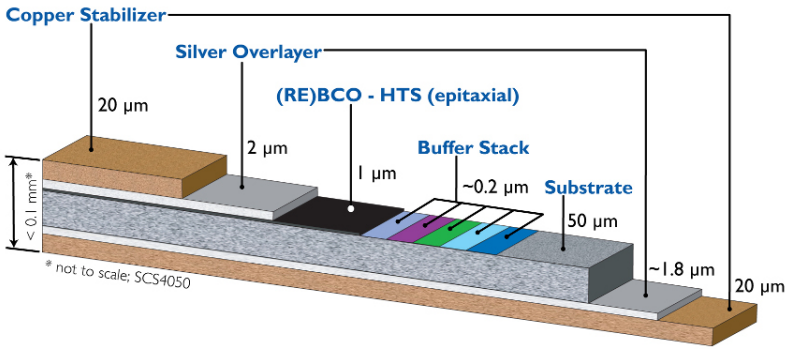


**Figure 5: Illustration of the structure of the YBCO tape by SuperPower. Source:** `http://www.superpower-inc.com/content/2g-hts-wire`

### Bi-2223/Ag Type HT and G from SEI

The Bi-2223 tapes produced by SEI are manufactured using the powder-in-tube method, where granulate precursor is placed in a tube of pure silver before heat

treatment, wire drawing and rolling. SEI's Bi-2223 type HT CETS 10-044-01 tape is reinforced by soldering the silver matrix in between two layers of copper alloy (thickness of 2x50 $\mu$m). The non-reinforced Bi-2223 Type G CETS 11-057-02 tape has a silver-gold alloy matrix Ag-Au5.4wt% to reduce thermal conductivity for current lead applications [15].

**OP processed Bi-2212/Ag wire**

The Bi-2212 PMM130723-2 wire by OST is produced by the PIT method. Granulate precursor supplied by Nexans SuperConductors GmbH is packed in a tube of silver, while the outer sheath of the wire is made of a Ag-0.2wt.%Mg alloy to provide reinforcement. The wire has 18 subelements, each containing 37 filaments (37x18 design). A Bi-2212 volume fraction was measured to be 22.1% after densification heat treatment by National High Magnetic Field Laboratory - Applied Superconductivity Center (NHMFL-ASC). Overpressure (OP) processing and heat treatment was done by NHMFL-ASC. A specialized heat treatment to optimize $I_c$ at 77 K was done by Nexans. Figure 6 shows a cross-sectional view of a Bi-2212 wire. This sample is further referred to by the designation: OP processed Bi-2212.

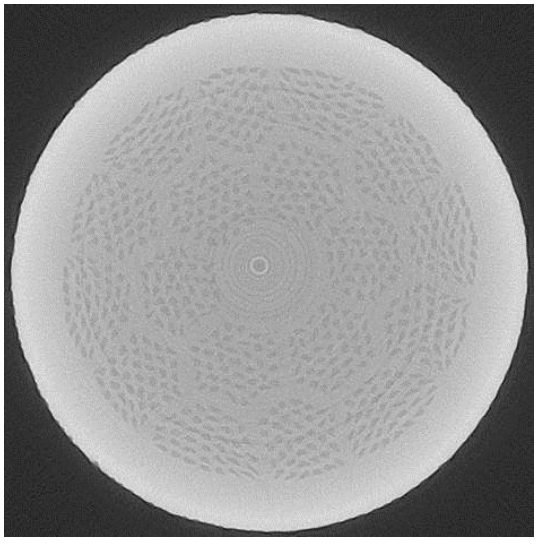

**Figure 6: Cross-sectional view of a overpressure processed Bi-2212 PMM130723-2 wire by OST. Courtesy: Christian Scheuerlein and Alexander Rack**

**Sample preparation**

Samples were cut to lengths of 150 mm for strain dependent critical current measurement. Four rectangular pieces of G10 plastic with dimensions 20x8x1mm were glued to the samples in order to avoid damaging the sample when clamping it in the tensile test machine and providing electrical insulation

during a critical current measurement. The glue used was EA-2A produced by Tokyo Sokki Kenkyujo Co. Ltd.

For the AMSC, SEI and OST samples the voltage taps were soldered on the tape using Kester 135 flux and 50In-50Sn solder at 150 °C. For the SuperPower sample the voltage taps were soldered using Sn62PbAg2 solder at 220 °C. Figure 7 shows a schematic view of a wire sample with G10 plastic insulation and instrumented with voltage taps.

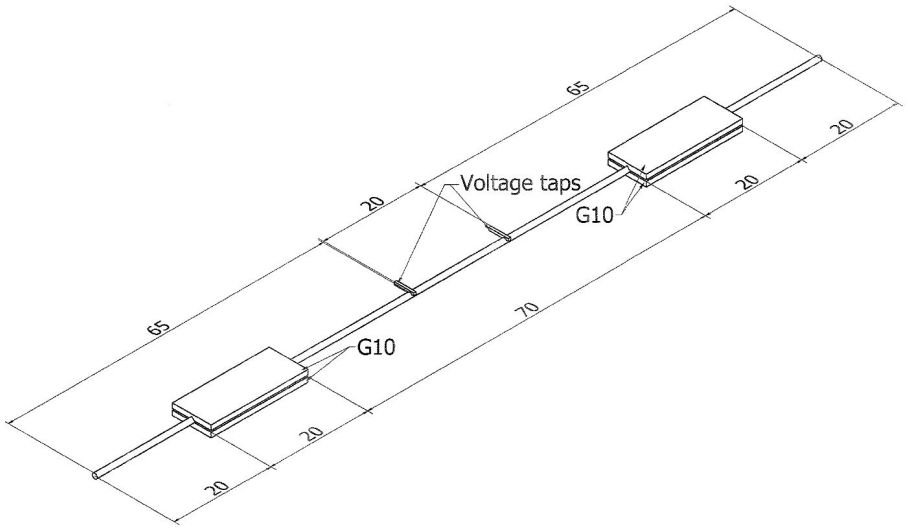


**Figure 7: Schematic view of instrumented wire, illustrating the positioning of G10 plastic and voltage taps**

## 3.3 Test procedures

A commercial universal test machine (UTM) and clip-on extensometer were used to characterize the mechanical properties of sample materials. The UTM was modified by mounting a reverse frame which allowed for tests on samples immersed in $LN_2$, in a open dewar. The extensometer was calibrated at ambient temperature and in $LN_2$. Then the tensile test set-up was used to perform strain dependent critical current measurements. Figure 8 (a) shows an instrumented YBCO sample mounted in the experimental set-up for strain dependent critical current measurement. The clip-on extensometer and current leads are seen mounted on the YBCO sample in Figure 8 (b). Figure 8 (c) shows the dewar lifted to immerse the sample in $LN_2$ for the duration of the tests.

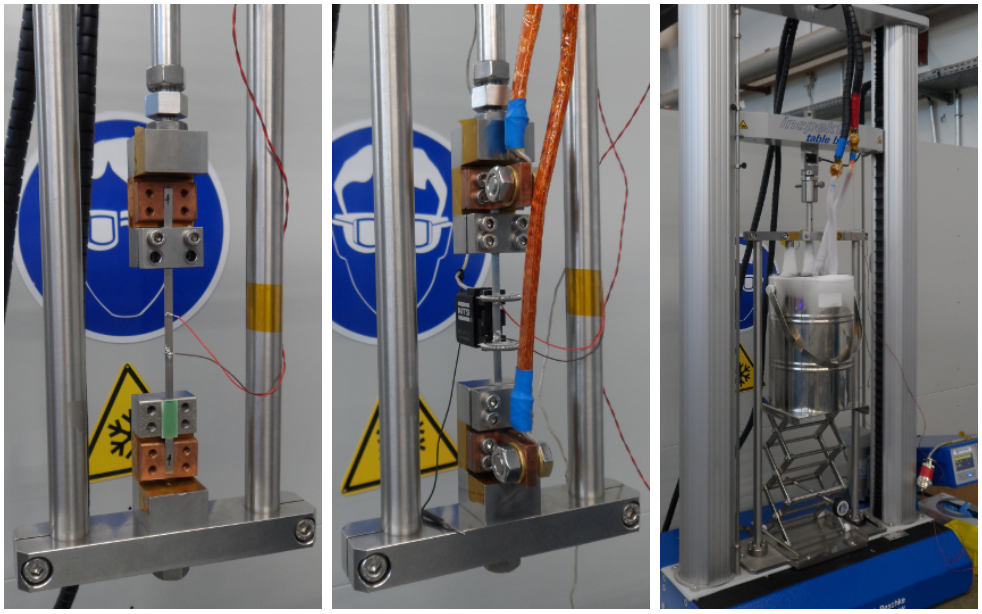

(a) (b) (c)

**Figure 8: Mounting arrangement of a AMSC YBCO tape sample during a $I_c(\varepsilon)$ measurement. (a) Sample mounted in upper grip with voltage taps soldered. Distance between grips is 70 mm. (b) Current leads fixed on sample ends and extensometer mounted on the middle of the sample. (c) Sample holder is immersed in liquid nitrogen during testing.**

### 3.3.1 Stress-strain measurement at 77 K

Following is a description of the tensile test equipment and procedures, as well as the calibration of the extensometer in $LN_2$.

#### The universal test machine

The UTM was produced by Hegwald & Peschke GmbH (H&P) from their series: "Inspekt table BLUE 05". It had a load capacity of 5 kN. It was operated by a software developed by H&P called "*LabMaster*". The load cell was produced by Angewandte System Technik (AST) Gruppe and was of the type KAP-S, which could be used up to a maximum load of 1 kN, and had an accuracy of 0.1% [16]. Sample grips where current leads could be attached, and which provided electrical insulation to the rest of the machine were designed and supplied by KEK (see Figure 8 (a)).

#### MTS-clip on extensometer

The extensometer was of the type MTS-clip on, 632.27F-21, with a gauge length of 25 mm. It could be used at temperatures ranging from −269 °C to

65 °C [17, p. 39]. Equation 2 describes the strain ($\varepsilon$) as a function of extensometer displacement ($l_{measured}$), divided by the gauge length of the MTS-extensometer (25 mm) and the calibration factor ($CF$) described in the following paragraph.

$$\varepsilon = \frac{l_{measured} \cdot 100}{CF \cdot 25mm} \ [\%] \tag{2}$$

**Extensometer calibration**
The MTS-extensometer was calibrated at room temperature (RT) and 77 K using a special calibration tool developed by KEK (The High Energy Accelerator Research Organization, in Japan) (see Figure 9 (Left)) while immersed in $LN_2$. Figure 9 (Right) shows the MTS-extensometer mounted to the tool's spindle and anvil. The spindle is displaced from its initial position to 0.5 mm and returned in steps of 0.1 mm. The procedure was repeated four times and a comparison was made by plotting extensometer displacement as a function of true displacement by the calibration tool.

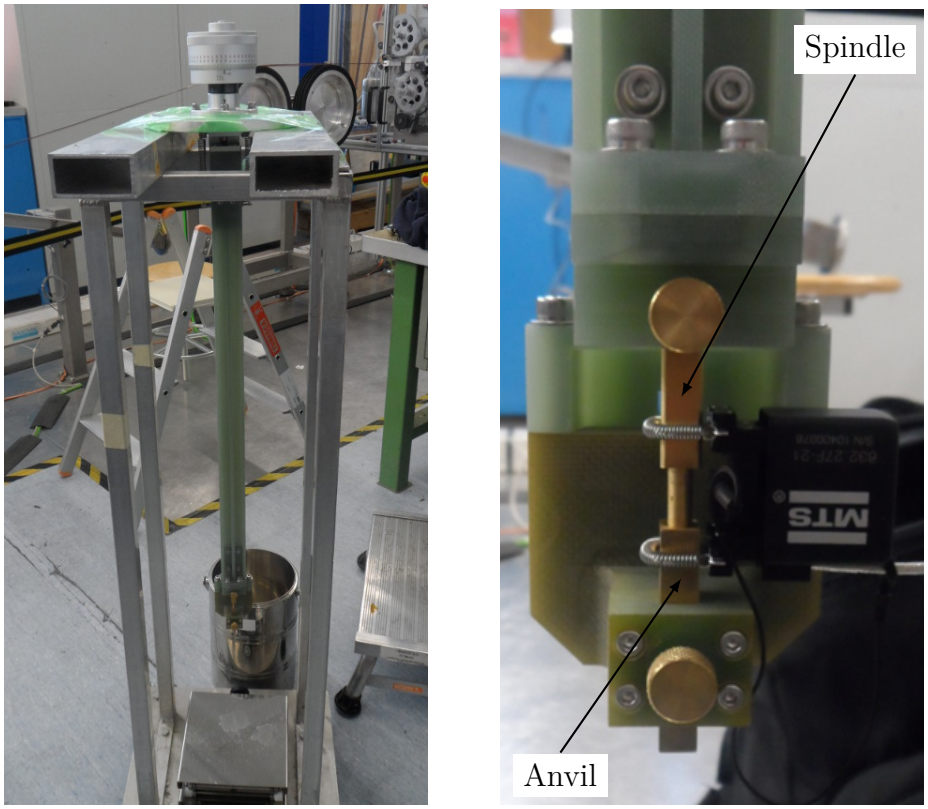


**(a)** **(b)**

**Figure 9: (a) Calibration tool set-up. (b) MTS-extensometer mounted on the anvil and spindle of the calibration tool**

The extensometer was initially calibrated at RT by the supplier, and the calibration presented here confirms the RT calibration. According to the linear fits made in Figure 10, the extensometer calibration factor (CF) at RT is practically 1, and at 77 K an extensometer displacement of 1.026 mm corresponds with a true displacement of 1.000 mm. Therefore, the measured displacement by the MTS-extensometer is divided by 1.026 in order to determine true displacement.

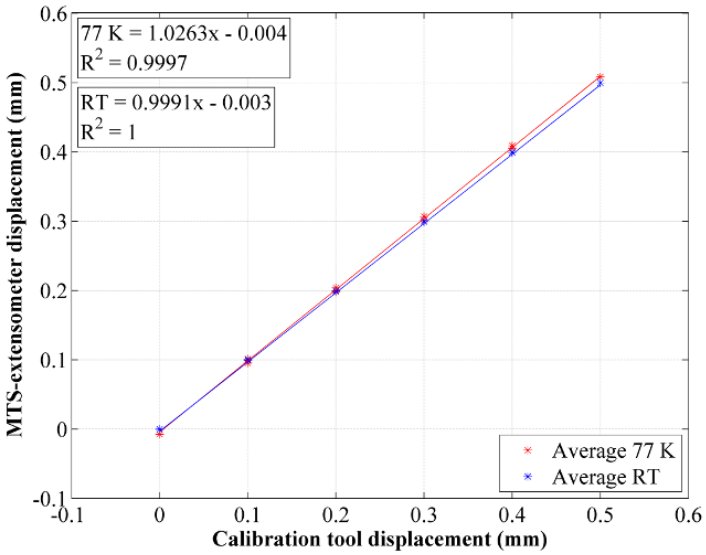


**Figure 10: Linear fit of the four MTS-extensometer displacement as a function of micrometer displacement recordings done at RT and 77 K**

### Comparison between MTS and Nyilas double extensometers

The strain reading of the MTS-extensometer was compared to that of a Nyilas double extensometers, seen in Figure 11 (a). The Nyilas double extensometers consists of two titanium frames, each holding four strain gauges connected to form a Wheatstone full-bridge. When the frames are deformed, half of the gages are compressed, and the other half are subjected to tensile strain. As a result of this, the collective system can determine sample strain on wires and tapes.

Figure 11 (b) shows a comparison of three engineering stress-strain acquired at RT, one of which was made with the MTS-extensometer and two made with the Nyilas double extensometer. The comparison shows that the MTS-extensometer's strain recording is nearly identical to that of the Nyilas double extensometers.

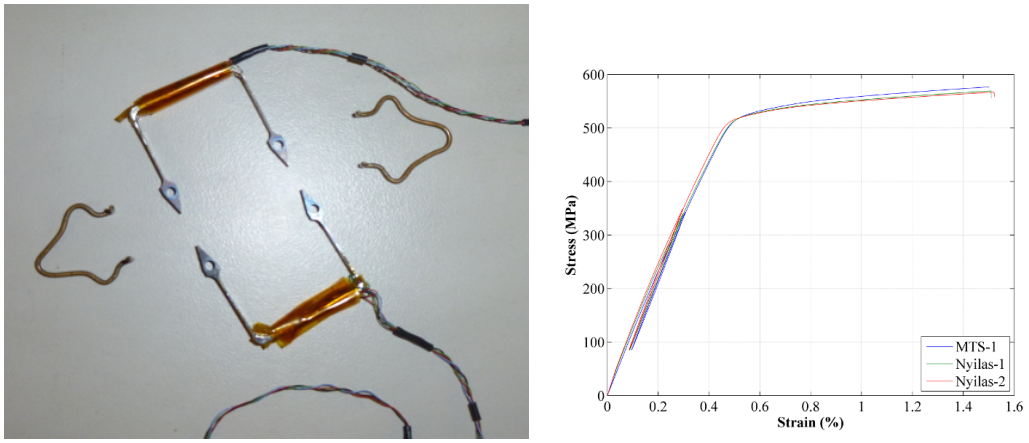


**(a)** **(b)**

**Figure 11: (a) Nyilas double extensometer and mounting spring. (b) A comparison of engineering stress-strain curves obtained from three samples of YBCO by SuperPower, one test using the MTS-extensometer and two tests Nyilas double extensometers at room temperature**

### Tensile test procedure

Samples were mounted in the grips vertically and straight in order not to introduce a bending moment. Measurements were conducted with a constant stroke rate equivalent to a strain rate of $10^{-4}$ $s^{-1}$ of an unstrained sample. A tensile pre-load was maintained on the samples during extensometer mounting and cool-down. Before initiating the loading, the extensometer strain was zeroed when the material is fully contracted as a result of the temperature gradient from RT to 77 K. The tensile tests were stopped before sample fracture in order to avoid damaging the extensometer.

### Engineering stress-strain curve

The load was recorded as a function of extensometer displacement. To determine the engineering stress, the applied force was divided by the original cross sectional area of the unloaded sample. The extensometer displacement was used to determine the percentage strain. The samples were unloaded at a pre-defined strain in order to determine $E_a$.

The initial portions of the engineering stress-strain curves of wires and tapes are not reproducible due to straightening of the sample during initial loading. As a result of this, a portion of the stress-strain curve is removed, as shown in Figure 12. The engineering stress-strain curve is shifted along the strain axis so that the linear loading lines intersects the (0, 0) point, by moving the strain contribution. This procedure was always executed prior to determining the mechanical properties.

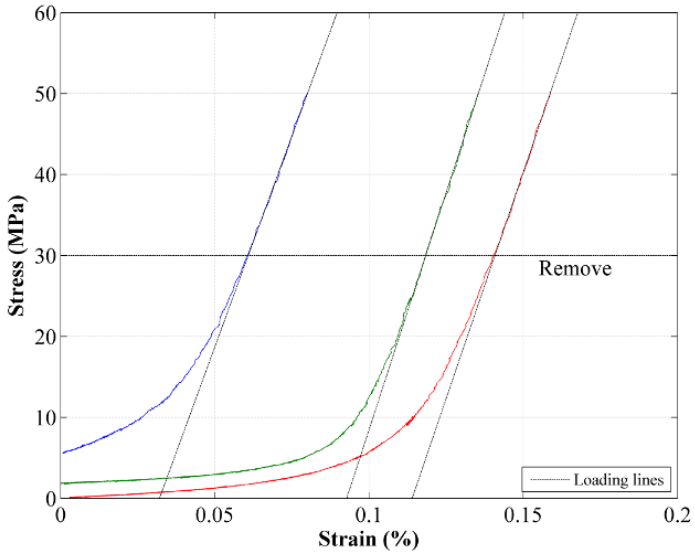


**Figure 12: Initial loading lines of three SuperPower YBCO samples. The low reproducibility is assumed to be due to straightening of the sample. The area of the engineering stress-strain curve which is below the horizontal line is removed and the strain axes of are moved so that the initial linear portion intersects the (0, 0) point.**

### 3.3.2 Critical current measurements

This section describes the instruments and procedure followed to measure $I_c$ using a four-point method. All $I_c$ measurements were conducted in liquid nitrogen and in self-field; the field generated when a current is passing through the conductor.

#### $I_c$ measurement set-up at CERN

The four-probe measurement system at CERN for critical current measurements in liquid nitrogen consists of a power supply of the type Genesys, GEN8-600, which has a voltage range of 0-8 V and current range of 0-600 A [18]. The multimeter is of the type PXI-4070 [19]. The current leads are rated for a minimum of 400 A.

#### Critical current measurement procedure

Figure 13 presents a schematic view of the four-point method used to measure the $I_c$, where a current ($I$) is induced to the sample and the resulting voltage potential is measured. The voltage was measured by wires soldered directly to the sample. As the generated voltage potential scales with the distance between the voltage taps, the electric field strength ($E$) is computed by dividing the voltage potential at any given point with the distance between the voltage

taps (20 mm). The $I_c$ is determined to be the current where the electric field criterion, defined as 1 $\mu$V/cm, intersects the *E-I* curve [10, p. 396]. The induced current is linearly increased until the electrical field strength surpasses 10 $\mu$V/cm.

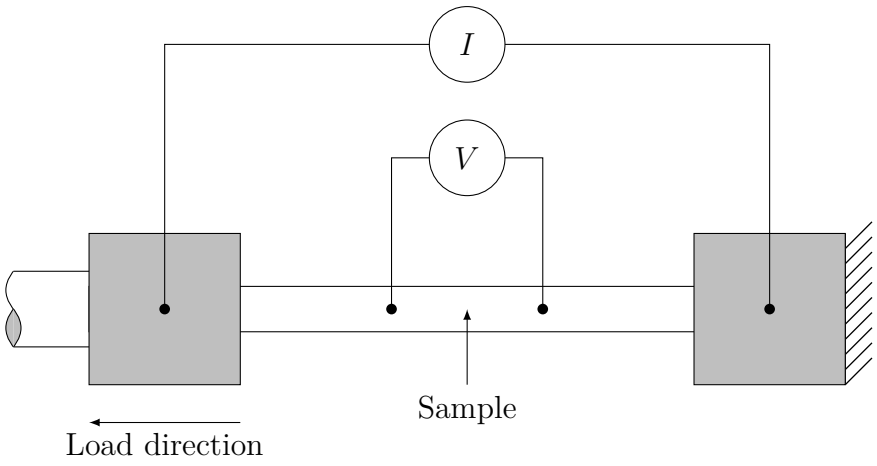


**Figure 13: Four-point method used to determine the critical current of a superconducting sample during tensile loading. While a strain is kept constant, a current is feed to the sample through current leads while the voltage potential is measured directly on the sample.**

Figure 14 shows the increase in electric field strength as a function of current. The *E-I* curve was fitted using a power law described below.

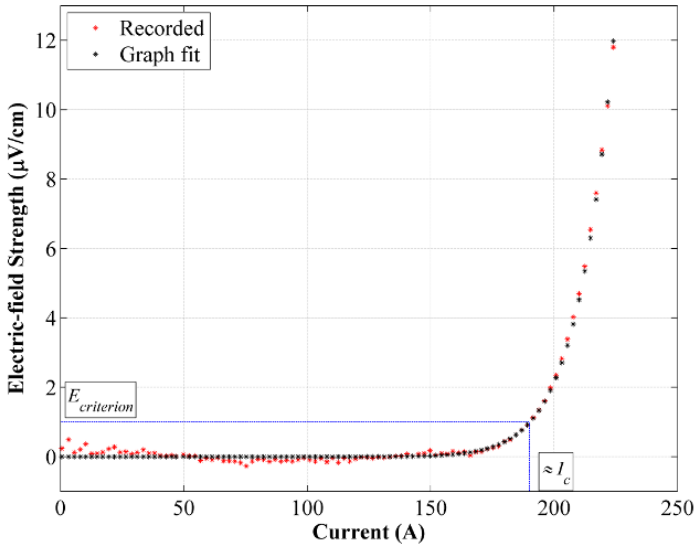


**Figure 14: The electric-field strength as a function of linearly increasing current of a Bi-2223 type HT tape by SEI at 77 K in self-field, and the resulting power law fit obtained from equation 3. $I_c$ is defined as the current where the electric field criterion of 1 $\mu V/cm$ intersects the *E-I* curve**

### Power law and least square method to determine the $I_c$ and *n-value*

A power law was used to determine the $I_c$ and *n-value* from an acquired *E-I* curve (see Equation 3). The *n-value* is the index of the fit which denotes the curves non-linearity. The curve was fitted in the region of the exponential growth where the measured electrical field strength was in the arbitrarily chosen range which includes the electrical field strength criterion from 0.3 to 10 $\mu V/cm$. The values of $I_c$ and *n-value* are tuned so that the sum of squared residuals ($SSR$)(see Equation 4) are minimized.

$$E_{c,i} = E_{criterion} \cdot \left(\frac{I_i}{I_c}\right)^n \tag{3}$$

*Where:*

| | |
|---|---|
| $E_{criterion}$ | is the electrical field criterion defined as 1 $\mu V/cm$ |
| $I_i$ | is the measured current at $i$ |
| $I_c$ | is the critical current |
| $n$ | is the index of non-linearity |

$$SSR = \sum_{i=1}^{n} (E_i - E_{c,i})^2 \tag{4}$$

*Where:*

| | |
|---|---|
| $E_i$ | is the measured electrical field strength at $i$ |
| $E_{c,i}$ | is the electrical field strength calculated from the power law |

**Strain dependent $I_c$ measurement procedure**
The UTM was used to strain a superconducting sample in order to measure the strain dependent $I_c$ ($I_c(\varepsilon)$) behavior. Before and during cool-down of a sample the UTM maintains a tensile pre-load to a sample. This pre-load is also the zero-strain load.

During the first $I_c$ measurement ($I_{c0}$), the UTM is in load control to hold the pre-load constant. After $I_{c0}$ was established, the UTM was instructed to increase the load until the extensometer measured the desired strain. When the target strain was reached the UTM was regulating the load to maintain the strain. At the target strain, the $I_c$ was measured, before the reloading. The load was periodically reversed to check if the $I_c$ was reversible, and to determine the $\varepsilon_{irr-5\%}$. This procedure was repeated until the superconducting properties of the samples dissipated or until fracture occurred. An $I_c$ measurement generally took about 5 minutes, from acquiring raw data, establishing the $I_c$ and straining to the next strain step.

## 3.4 Combined lattice parameter, stress, strain and critical current measurement at ID15B beamline at ESRF

Strain dependent critical current measurements combined with lattice parameter measurements were performed at the European Synchrotron (ESRF) ID15B beamline. The ID15B beamline is a high-energy scattering beamline that can provide a flux of high energy photos, required to penetrate the superconducting samples which are immersed in liquid nitrogen. The small scattering angle of the high-energy beamline enables fast non-destructive x-ray diffraction measurements during stress-strain $I_c$ measurements [20]. The beam had an energy of 86.9 keV and beam size of $0.2 \times 0.2$ $mm$ during the experiment. The diffraction images were acquired by a two dimensional Perkin Elmer XRD1621 CN3-ES detector.

In addition to the UTM, a mobile critical current measurement system was required for the $I_c(\varepsilon)$ measurements. An x-ray transparent cryostat, and a connecting plate to mount the UTM onto the xy sample translation stage in the ID15 beamline. Figure 15 shows the UTM mounted in the ID15B beamline at ESRF.

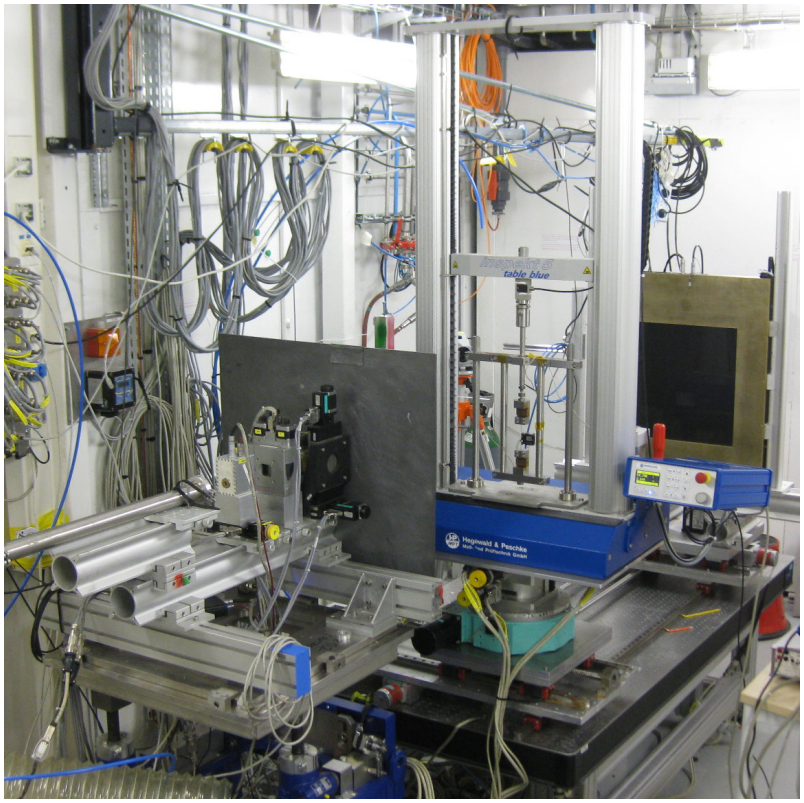

**Figure 15: Tensile test machine installed in the ID15 beamline of ESRF**

### 3.4.1 Critical current measurement system

The instruments required for the critical current measurement were a power supply, power supply control unit and a multimeter.

**Power supply:** Delta elektonika SM6000-series, model: SM30-200. The unit can supply a voltage of 0-30V, and current of 0-200A.

**Power supply controller:** Delta elektronika PSC-488 interface.

**Multimeter:** Keithley model 2001 digital multimeter 7-½ digit.

Figure 16 shows how the critical current test equipment was connected. The PSC-488 and Kiethley multimeter communicated with a computer through a GBIP to USB cable. Communication between the PSC-488 and the power supply was done through a standard analogue 15-pin cable.

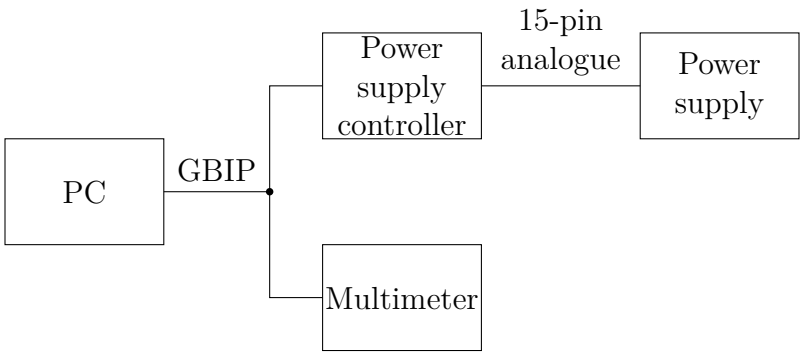


**Figure 16: Diagram showing the type of connection between the instruments used in a four-point measurement.**

### Critical current measurement software

The software used to control the power supply and read the multimeter was programmed in LabVIEW. Figure 17 shows a basic flowchart of the operations which the software had to perform. When the program is initiated the power increments by the pre-defined step. The current and voltage is measured every time the current is increased, all the while controlling if the target value of current is reached. If the target current is reached, the program stops. After 1 second, the program reverts to the start and the current is incremented once more.

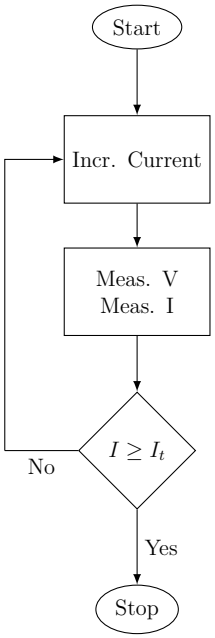


**Figure 17: Flow chart of the LabVIEW program developed to record the V-I characteristics of a conductor. The induced current and voltage potential is measured each time the current is incremented. The cycle is stopped when the targeted current is reached, or if the system is manually stopped.**

Figure 19 shows the front panel of the LabVIEW software. Following is a list describing the in- and outputs.

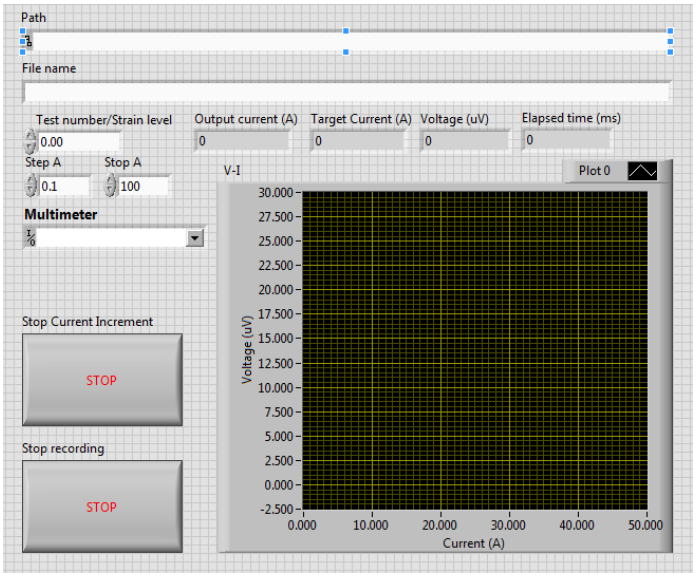


**Figure 18: Front panel of the software developed to control the current ramp and acquiring a *V-I* curve.**

**Path:** inputs the path where the resulting file will be generated.

**File name:** inputs the name of the file that will be generated.

**Test number/Strain level:** inputs the test number or strain level which indicates the current measurement being done. This string is added to the resulting file name.

**Step A and Stop A:** inputs the current step and the current at which the ramp will cease, respectively.

**Multimeter:** inputs the address to the multimeter.

**Stop current increase/recording:** boolean input which is used to manually stop the current ramp or *V-I* recording, respectively.

**Output current (A):** shows the measured current in amperes at the point *i*.

**Target current (A):** shows the target current in amperes at the point *i*.

**Voltage (uV):** shows the measured voltage potential at the point *i*.

**Elapsed time (ms):** shows the elapsed time in milliseconds since the program was initiated.

The resulting ASCII text file is generated after recording stops, and can be opened in Microsoft Excel for analysis. Figure 19 shows the raw *V-I* data acquired for one sample of superconducting wire. Column *A* hold the elapsed time in milliseconds while columns *B* and *C* holds the measured current in amperes and voltage potential in microvolt, respectively.

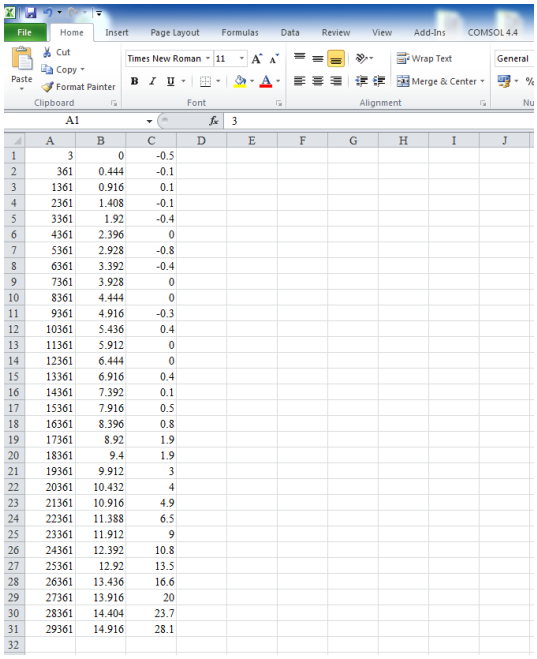

| | A | B | C |
|---|---|---|---|
| 1 | 3 | 0 | -0.5 |
| 2 | 361 | 0.444 | -0.1 |
| 3 | 1361 | 0.916 | 0.1 |
| 4 | 2361 | 1.408 | -0.1 |
| 5 | 3361 | 1.92 | -0.4 |
| 6 | 4361 | 2.396 | 0 |
| 7 | 5361 | 2.928 | -0.8 |
| 8 | 6361 | 3.392 | -0.4 |
| 9 | 7361 | 3.928 | 0 |
| 10 | 8361 | 4.444 | 0 |
| 11 | 9361 | 4.916 | -0.3 |
| 12 | 10361 | 5.436 | 0.4 |
| 13 | 11361 | 5.912 | 0 |
| 14 | 12361 | 6.444 | 0 |
| 15 | 13361 | 6.916 | 0.4 |
| 16 | 14361 | 7.392 | 0.1 |
| 17 | 15361 | 7.916 | 0.5 |
| 18 | 16361 | 8.396 | 0.8 |
| 19 | 17361 | 8.92 | 1.9 |
| 20 | 18361 | 9.4 | 1.9 |
| 21 | 19361 | 9.912 | 3 |
| 22 | 20361 | 10.432 | 4 |
| 23 | 21361 | 10.916 | 4.9 |
| 24 | 22361 | 11.388 | 6.5 |
| 25 | 23361 | 11.912 | 9 |
| 26 | 24361 | 12.392 | 10.8 |
| 27 | 25361 | 12.92 | 13.5 |
| 28 | 26361 | 13.436 | 16.6 |
| 29 | 27361 | 13.916 | 20 |
| 30 | 28361 | 14.404 | 23.7 |
| 31 | 29361 | 14.916 | 28.1 |
| 32 | | | |

**Figure 19: Raw data acquired by the LabVIEW program is exported to Excel. Column *A* hold the elapsed time in milliseconds while columns *B* and *C* holds the measured current in amperes and voltage potential in microvolt, respectively.**

### Test of software

The functionality of the system was controlled by obtaining *V-I* curves from one sample of superconducting YBCO tape by SuperPower, immersed in liquid nitrogen. Figure 20 shows 12 *E-I* curves where the voltage potential is converted to the electrical field strength between the voltage taps.

The YBCO sample by SuperPower was prepared by soldering the voltage taps to the tape using Sn62PbAg2 solder at 235 °C, and ERAMA 5 flux.

The *E-I* curves showed very good reproducibility, and after conducting a power law fit the $I_c$ is determined to be $137.7 \pm 0.4$ A using an electrical field strength criterion of 1 $\mu V/cm$, at 77 K in self-field.

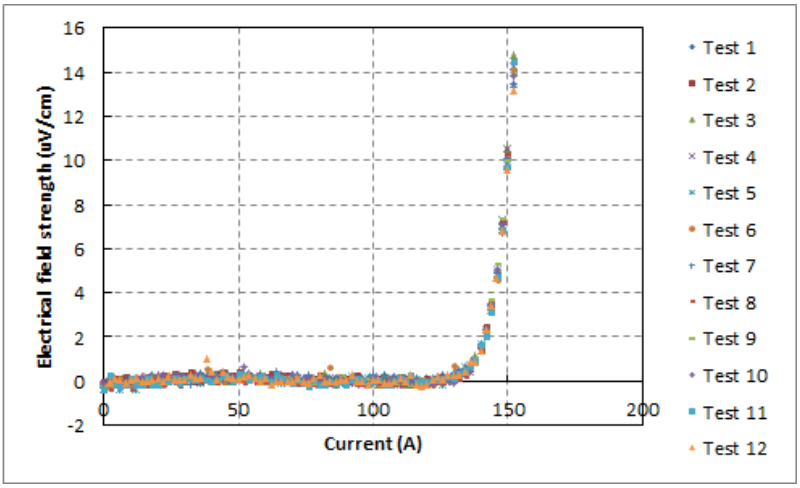


**Figure 20: Comparison of 12 *E-I* curves from a superconducting YBCO tape by SuperPower acquired by the LabVIEW program. The curves obtained using the new measurement system produces a well reproducible results, and the $I_c$ is determined to be $137.7 \pm 0.4$ A at 77 K in self-field.**

### 3.4.2 Integration of the UTM in the ID15B beamline

For the integration of the UTM in the ID15B beamline an connecting plate and an X-ray transparent cryostat had to be developed. All technical drawings are given in appendix C.

#### Connecting plate

A connecting plate was required to mount the UTM on the translation stage that moves the sample in the horizontal x and y directions. The xy-stage was of the type Huber series 5102.20. The connecting plate's dimensions equals the footprint of the UTM and follows the specifications of the xy-stage given in the Huber user's manual [21]. Since the maximum load on the Huber xy-stage is approximately 100 kg, the connecting plate was made of 10 mm thick aluminium to limit weight.

#### Cryostat

A new cryostat was required for the synchrotron experiments for two reasons. It was necessary to minimize the absorption of the synchrotron beam in the cryostat walls and in the liquid nitrogen. Secondly, it was impossible to lift a cryostat and immerse a sample in liquid nitrogen as shown in Figure 8 (c), since the vertical distance from the xy-stage (onto which the UTM is mounted) to the beam in the ID15B-beamline is 275±20 mm. Therefore, the columns supporting the reverse frame were shortened in order to mount the sample as close to the UTM-base as possible. The cryostat is designed to have the ability of being split longitudinally, and assembled around the frame of the sample

holder.

The cryostat was made of 1 mm thick sheets of stainless steel, encapsulated with styrofoam. The chosen material for the windows is a 0.35 mm thick sheet of Polyethylene terephthalate (PET). CAF4 silicone is used to join the windows and the stainless steel surface in order to produce a leakproof join.

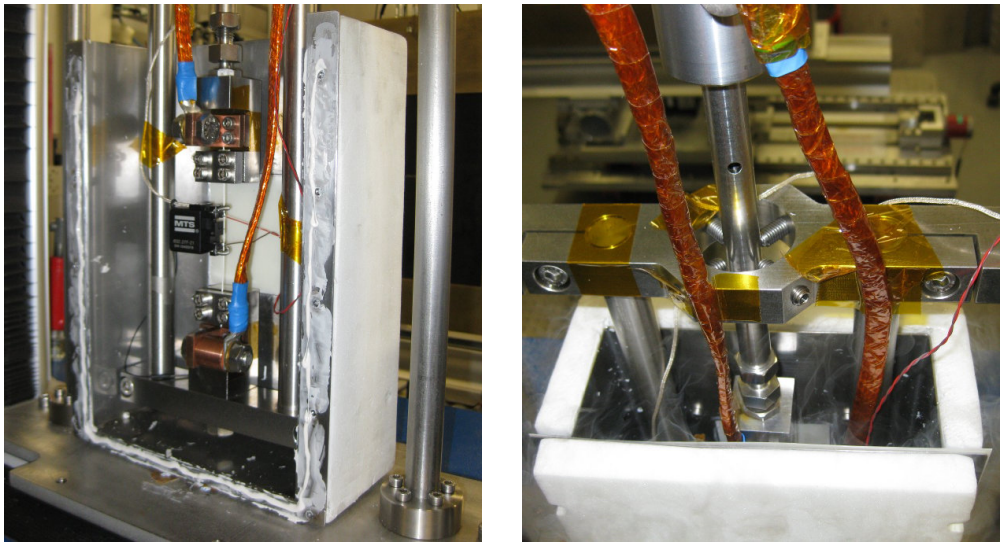

**(a)** **(b)**

**Figure 21: (a) The cryostat half-assembled in the ID15B beamline, during preparation for a critical current measurement at 77 K. (b) Top view of the sealed cryostat partially filled with $LN_2$ during a critical current measurement.**

Figure 21 (a) shows the cryostat half-assembled in the ID15B beamline, during preparation for a critical current measurement at 77 K. Figure 21 (b) shows the top view of the sealed cryostat, partially filled with $LN_2$.

The opened cryostat required a refill approximately every 20 minutes, which was sufficiently long to conveniently conduct the experiments described below.

### 3.4.3 Procedure for acquiring and evaluating 2D-diffraction images

X-ray diffraction measurements were performed in transmission geometry, which means that the detector is placed behind the sample. The 2-dimensional detector acquires an image of the X-rays that were diffracted in the sample. A diffraction pattern is shown in Figure 22. During the simultaneous lattice parameter, critical current stress and strain measurements a diffraction image was acquired at each strain step where $I_c$ was measured.

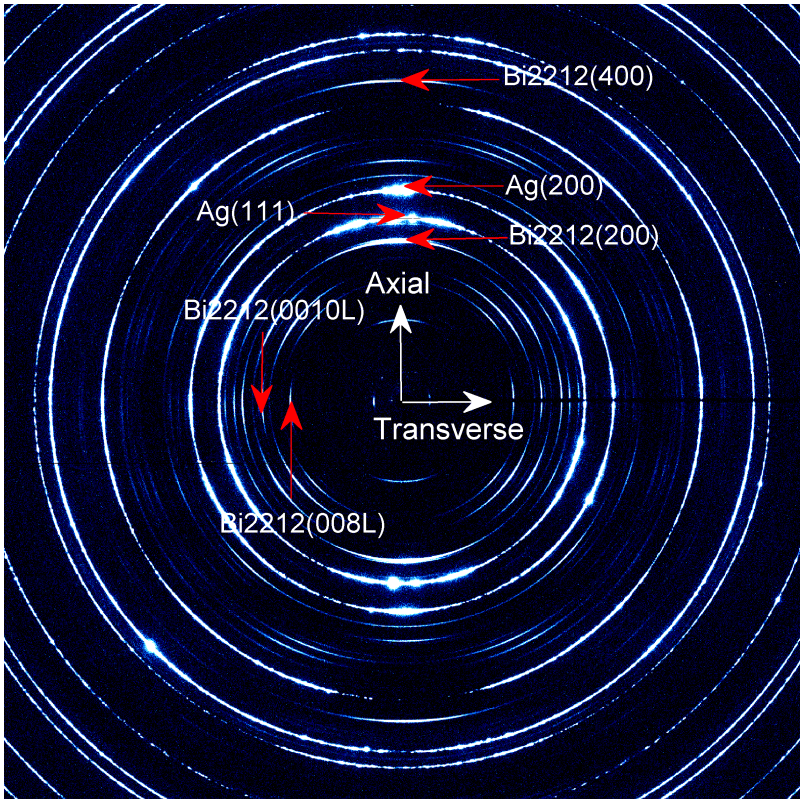


**Figure 22: Diffraction image acquired in transmission geometry at RT**

The diffraction images were segmented at 0, 90, 180 and 270 degrees in 15° slices before radial integration (see Figure 22). Segmentation and radial integration of the diffraction pattern was done using the ESRF FIT2D software [22]. 0° and 180° is the axial direction of the wire, while 90° and 270° is the transversal direction of the wire.

A Gaussian function was fitted in order to determine the *d-spacing*. The relative change in lattice *d-spacing* of the superconducting material was normalized to the *d-spacing* of the unstrained sample. The resulting relative *d-spacing* was plotted as a function of measured wire strain by the extensometer. Figure 23 shows an example of a fitted Bi-2212(200) peak for the OP processed Bi-2212 wire by OST at RT.

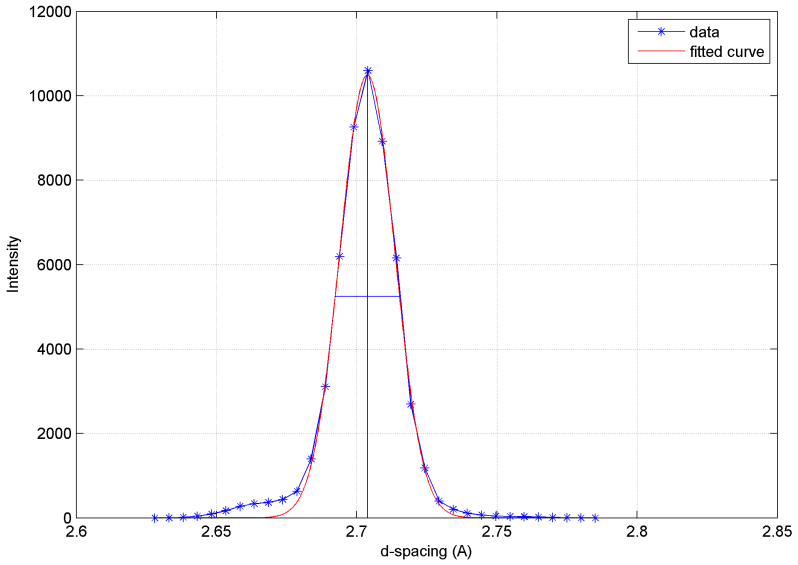


**Figure 23: Example of a fitted Bi-2212(200) peak using a Gaussian function.**

# 4 Results

## 4.1 Mechanical properties at 77 K

The mechanical properties of the YBCO, Bi-2223 and Bi-2212 samples were characterized at 77 K on three samples of each type. Figure 24 shows a comparison of the different HTS samples characterized at 77 K. The YBCO tapes exhibited the highest strength due to the substrate materials, Hastelloy C-276 in the SuperPower and Ni-5%at.W in the AMSC tape. The non-reinforced (Type G) and the reinforced (Type HT) Bi-2223 tapes rupture at a strain of roughly 0.2% and 0.4%, respectively. Fracture occurred at the grips, presumably due to stress concentrations. The OP processed Bi-2212 wire has the lowest ultimate strength, but ruptures at much higher strain than the Bi-2223 tapes.

All engineering stress-strain curves are presented in appendix B.

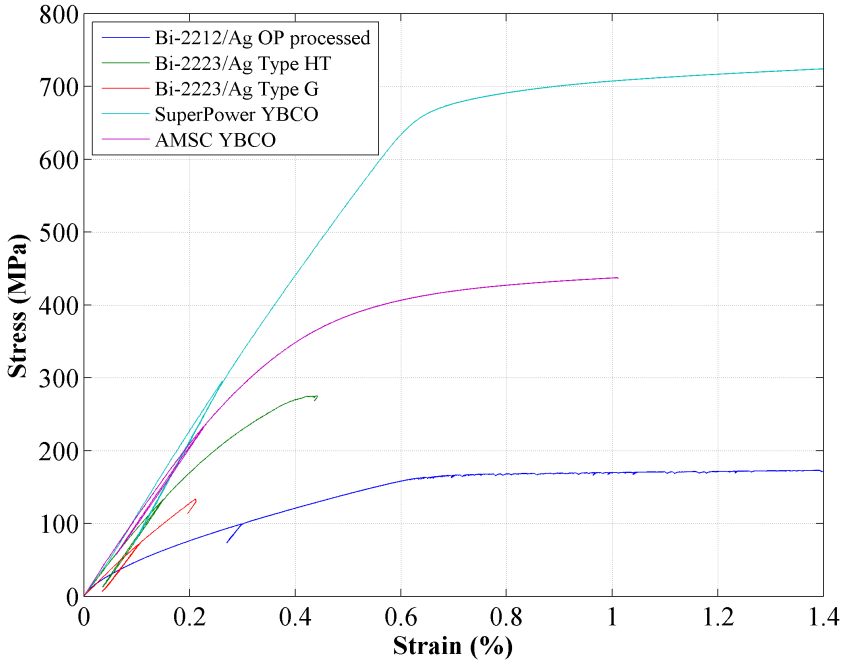


**Figure 24: Comparison of the stress-strain curves acquired for for different HTS at 77 K. The initial portion of the curves are fitted using a linear or polynomial regression, then shifted along the strain axis so that the curve intersects the (0,0) point.**

Table 2 summarizes the average values for moduli of elasticity, offset yield strength and strain, maximum tensile stress and strain obtained during the

mechanical characterization.

**Table 2: Summary of average values for $E_a$, $R_{p0.2}$, $\varepsilon_{p0.2}$, $R_{max}$ and $\varepsilon_{max}$ for the different HTS. *Tensile test was stopped at recorded value. **A 0.2% offset yield strength could not be determined and is replaced with 0.02% offset yield strength.**

| Sample | $E_a$ (GPa) | $R_{p0.2}$ (MPa) | $\varepsilon_{p0.2}$ (%) | $R_{max}$ (MPa) | $\varepsilon_{max}$ (%) |
|---|---|---|---|---|---|
| AMSC YBCO | $109 \pm 2.7$ | $408 \pm 3.5$ | $0.57 \pm 0.01$ | >429* | >1.0* |
| SuperPower YBCO | $132.5 \pm 1.3$ | $676 \pm 6.3$ | $0.72 \pm 0.02$ | >713* | >1.4* |
| SEI Bi-2223 type HT | $104 \pm 3.8$ | $120.7 \pm 7.7$** | $0.14 \pm 0.01$** | $268 \pm 6.0$ | $0.41 \pm 0.02$ |
| SEI Bi-2223 type G | $98.0 \pm 2.2$ | $54.6 \pm 0.9$** | $0.08 \pm 0.00$** | $126 \pm 6.4$ | $0.20 \pm 0.01$ |
| OP processed Bi-2212 | $94.5 \pm 7.6$ | $104 \pm 5.3$ | $0.31 \pm 0.01$ | >178* | >3.8* |

## 4.2 Strain dependent $I_c$ degradation at 77 K in self-field

### AMSC YBCO tape

The electromechanical properties of the AMSC YBCO tape were determined by performing tensile tests on three samples, and strain dependent critical current measurements on two samples.

Figure 25 shows the relative critical current degradation as a function of applied tensile strain. The $I_c$ values of the unloaded samples were determined to be 112 and 109 A, respectively. For sample 1, when a strain of 0.42% was reached, the load was periodically reversed and $I_c$ was remeasured at a strain 0.09% lower. Sample 2 was periodically returned by 0.08% strain after reaching a strain of 0.72%. For sample 1 and sample 2 the irreversible strain limit was determined to be 1.07% and 1.03%, respectively.

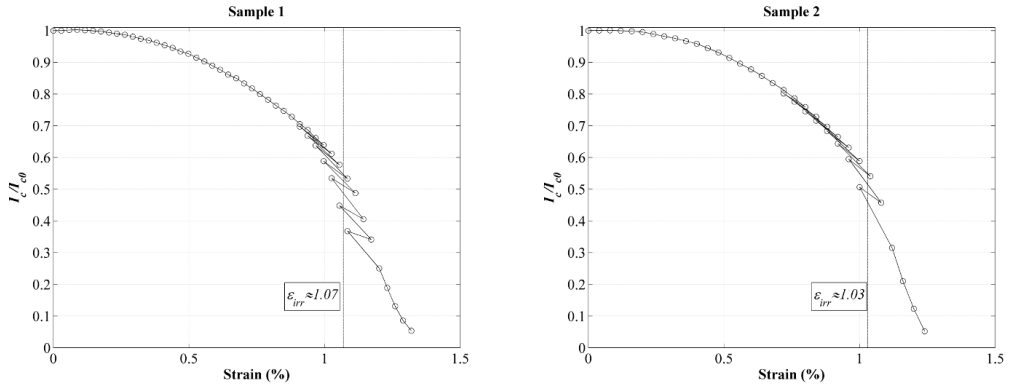


**Figure 25: Relative $I_c$ degradation as a function of strain for two samples of YBCO tapes by AMSC at 77 K in self-field**

The $I_c$ and *n-value* variation as a function of tensile strain of two YBCO tape samples by AMSC is presented in Figure 26. It can be seen that the $I_c(\varepsilon)$ measurements are well reproducible, with a 95% reversible retention of $I_c$ at strains of 0.43% and 0.42% for sample 1 and sample 2, respectively. A strong reduction in *n-value* occurs when $\varepsilon_{irr-5\%}$ is exceeded.

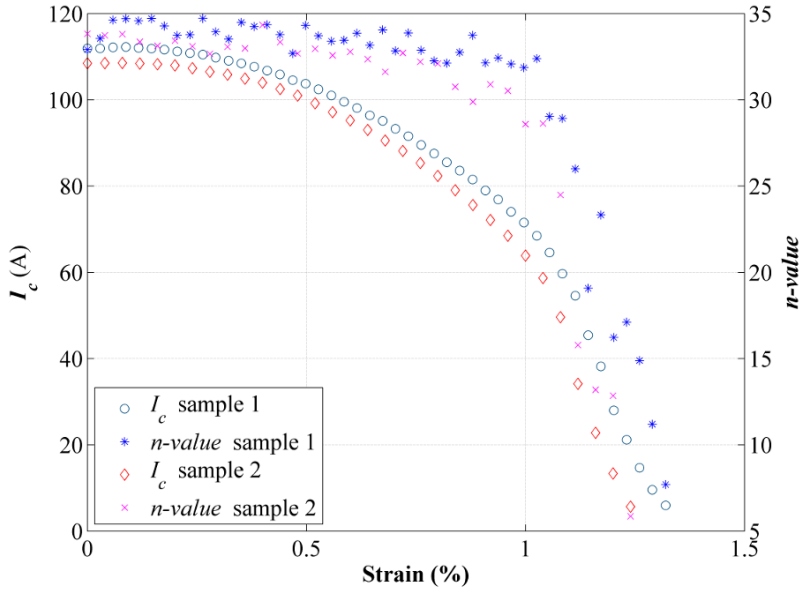


**Figure 26: Reduction in $I_c$ and *n-value* as a function of applied tensile strain for two samples of YBCO tapes by AMSC at 77 K in self-field.**

### SuperPower YBCO tapes

The electromechanical properties of the SuperPower YBCO tape were determined by performing tensile tests on three samples, and strain dependent critical current measurements on one sample.

Figure 27 shows the relative $I_c$ degradation as a function of applied tensile strain of one YBCO tape by SuperPower. Return points lower than 0.54% were excluded from the graph in order to concentrate the attention to the region of interest.

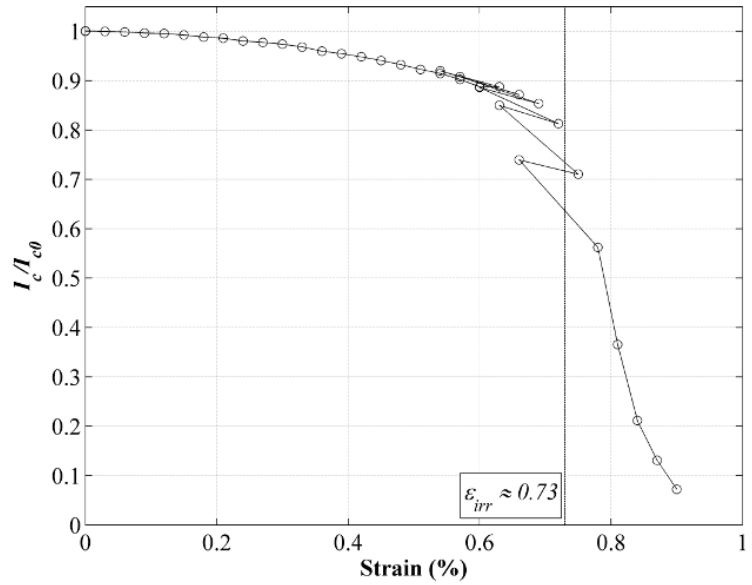


**Figure 27: Relative $I_c$ degradation as a function of strain for the SuperPower YBCO tape at 77 K in self-field.**

Figure 28 shows the $I_c$ and *n-value* variation as a function of tensile strain. The $I_c$ of the unloaded sample was determined to be 122 A. The strain where a 95% reversible retention of $I_c$ and the irreversible strain limit is determined to be 0.44% and 0.73%, respectively. There is a sharp drop in $I_c$ after 0.6%, which corresponds to the strain where a plateauing in the $\sigma(\varepsilon)$ curves observed in Figure 24.

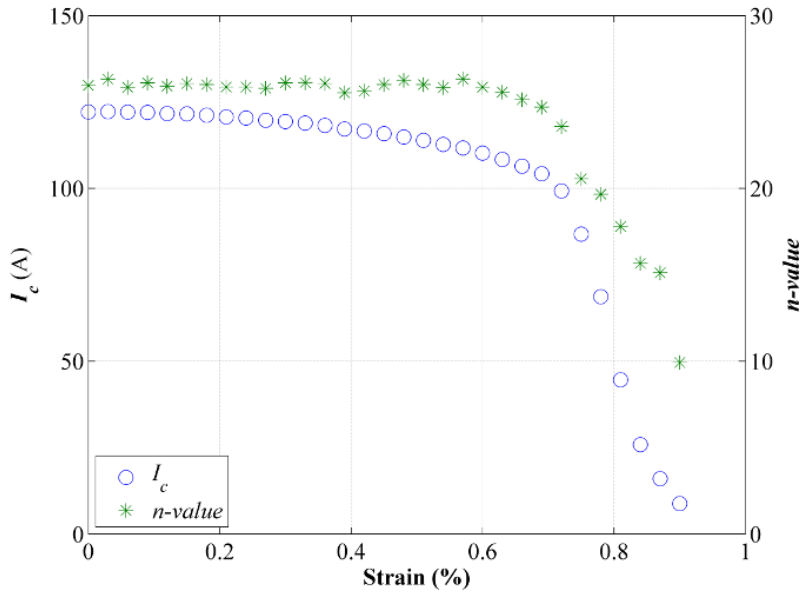


**Figure 28: Reduction in $I_c$ and *n-value* as a function of applied tensile strain of the SuperPower YBCO tape at 77 K in self-field.**

### SEI Bi-2223 type HT tapes

The electromechanical properties of the SEI Bi-2223 tape types HT were determined by performing tensile tests on three samples, and strain dependent critical current measurements on two samples.

The relative reduction in $I_c$ as a result of applied tensile strain is presented in Figure 29. Both samples were strained by 0.02% increments between each $I_c$ measurement. A 95% retention of $I_c$ or an irreversible strain limit was not observed before the samples fractured at 0.40% and 0.44% strain for sample 1 and sample 2, respectively. Therefore, return-points are not added to the graphs presented below.

The $I_c$ and *n-value* variation as a function of tensile strain of the Bi-2223 type HT tapes are shown in Figure 30. It can be seen that the $I_c(\varepsilon)$ measurements with the SEI type HT are well reproducible.

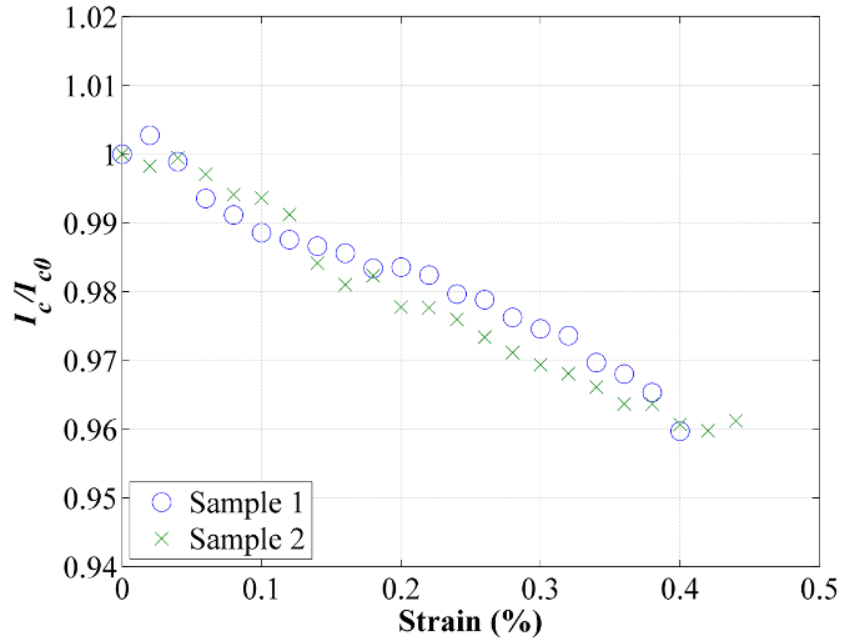


**Figure 29: Relative $I_c$ degradation as a function of strain for two samples of Bi-2223 type HT by SEI at 77 K in self-field**

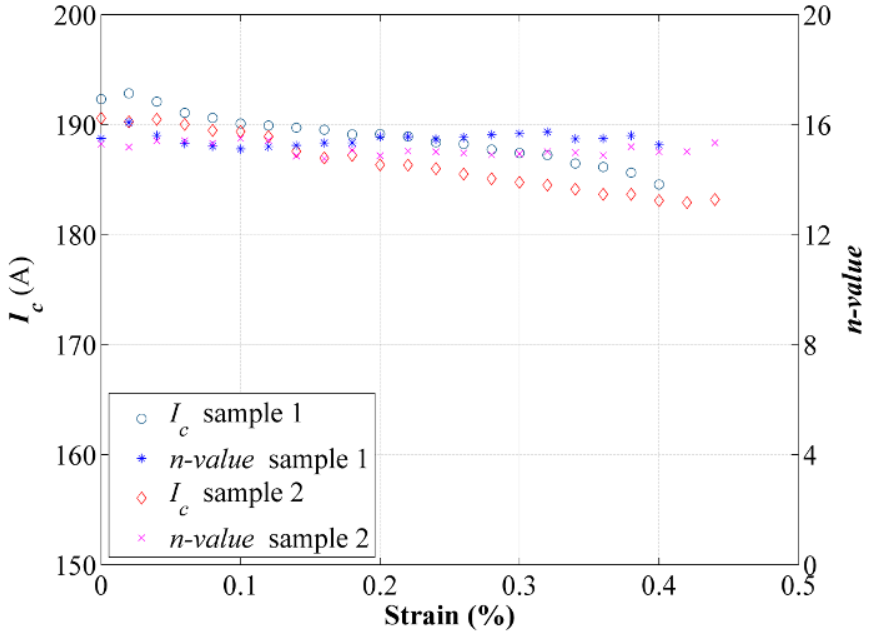


**Figure 30: Reduction in $I_c$ and *n-value* as a result of applied tensile strain for two samples of Bi-2223 type HT by SEI tape at 77 K in self-field.**

**SEI Bi-2223 type G tapes**
The electromechanical properties of the SEI Bi-2223 type G tapes were determined by performing tensile tests on three samples, and strain dependent critical current measurements on two samples.

The relative reduction in $I_c$ as a result of applied tensile strain is presented in Figure 31. Both samples were strained by 0.01% increments between each $I_c$ measurement. A 95% retention of $I_c$ or an irreversible strain limit was not observed before the samples fractured at 0.17% and 0.20% strain for sample 1 and sample 2, respectively. Therefore, return-points are not added to the graphs presented below.

The $I_c$ and *n-value* variation as a function of tensile strain of the Bi-2223 type G are shown in Figure 32. It can be seen that the $I_c(\varepsilon)$ measurements with the Bi-2223 type G are well reproducible.

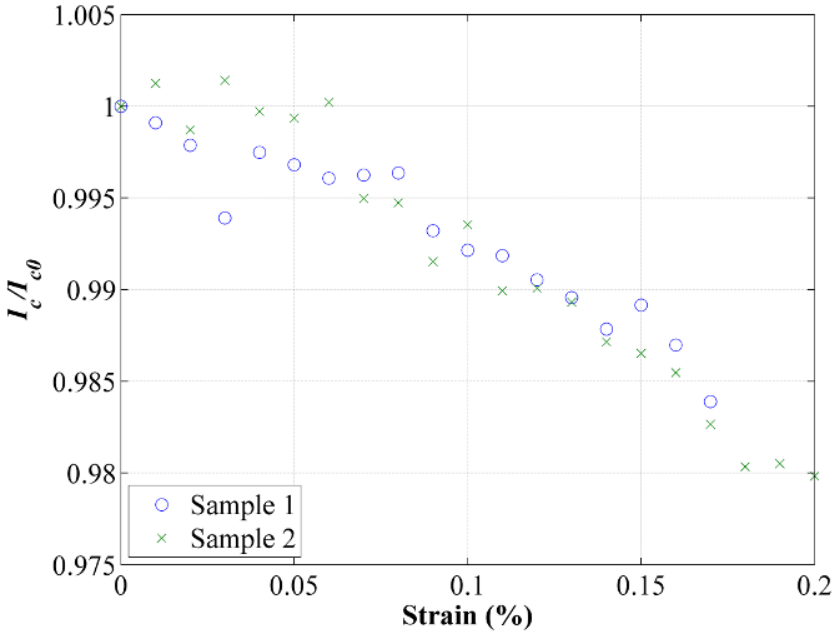


**Figure 31: Relative $I_c$ degradation as a function of strain for two samples of Bi-2223 type G by SEI at 77 K in self-field**

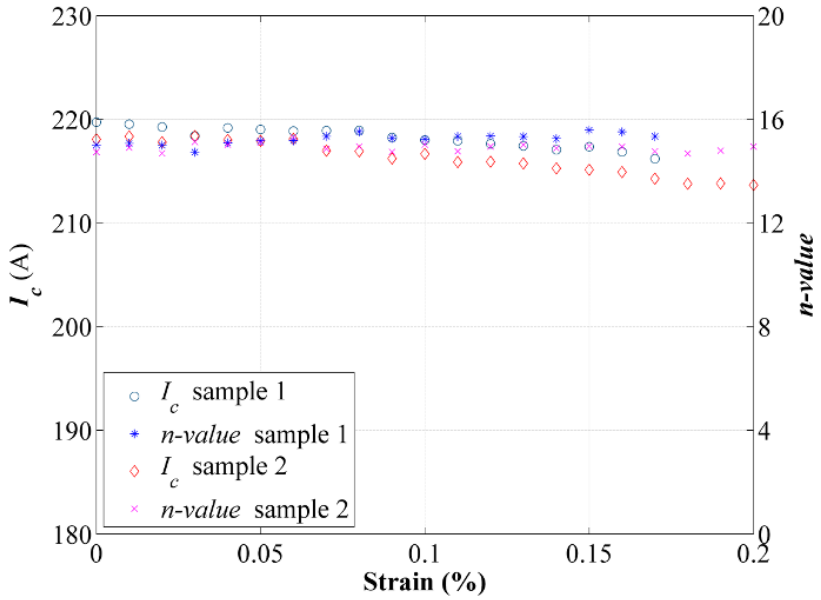


**Figure 32: Reduction in $I_c$ and *n-value* as a result of applied tensile strain for two samples of Bi-2223 type G by SEI at 77 K in self-field.**

### OP processed Bi-2212 wire

The electromechanical properties of the OP processed Bi-2212 wires were determined by performing tensile tests on four samples, and strain dependent critical current measurements on three samples.

$I_c$ as a function of applied tensile strain for the three samples are presented in Figure 33 (a). For sample 1 and 3 the increase in strain remained constant by 0.02%, while sample 2 increased by 0.05% strain between each $I_c$ measurement. 33 (b) show the comparison of three stress-strain curves obtained during uniaxial tensile tests at 77 K and three stress-strain-*n-value* curves obtained during $I_c(\varepsilon)$ measurements at 77 K in self-field. A strong reduction in $I_c$ and *n-value* is observed after 0.65% strain, most likely due to filament cracking. Filament fracturing can also explain the plateauing in the engineering stress-strain curves in Figure 33 (b).

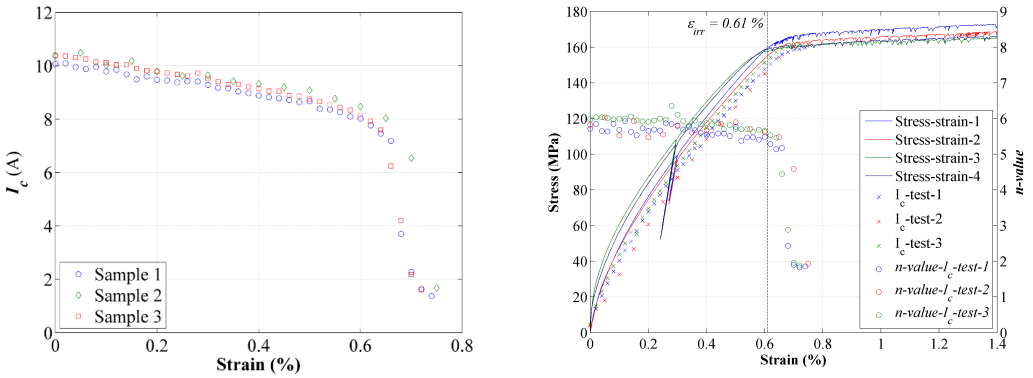


**(a)** **(b)**

**Figure 33: (a) $I_c$ degradation as a function of wire strain. (b) Summary of the Bi-2212 wire stress-strain and *n-value* vs strain curves acquired at 77 K.**

Sample 1 was partially unloaded by returning the strain by 0.08% before re-measuring the $I_c$. Sample 2 was completely unloaded by returning the load to the initial pre-load of 2 N after each strain-step. Figure 34 (a) shows the relative $I_c$ degradation of sample 2. An irreversible strain limit was observed at 0.62% and 0.60% for sample 1 and 2, respectively. A $\varepsilon_{95\%}$ was observed at 0.20%, 0.22% and 0.19% for sample 1, 2 and 3, respectively. Figure 34 (b) shows the permanent wire elongation (plastic deformation) of sample 2 after returning the load to the pre-load.

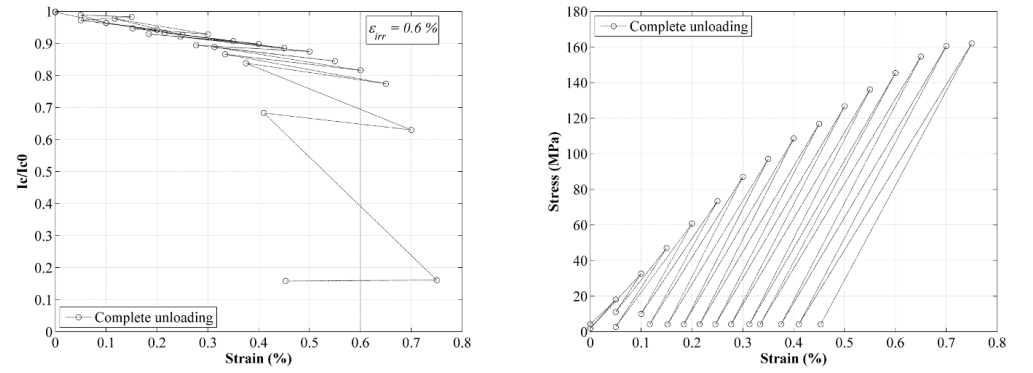


**(a)** **(b)**

**Figure 34: (a) Self-field critical current at 77 K as a function of strain. (b) Permanent wire elongation after stress relaxation as a function of the maximum wire stress.**

## Summary

Table 3 summarizes the critical current of the unloaded samples ($I_{c0}$), the

strain where a 95% $I_c$ retention is observed ($\varepsilon_{95\%}$), the irreversible strain limit ($\varepsilon_{irr-5\%}$) and the irreversible *n-value* reduction of 10% ($\varepsilon_{n\text{-}value\text{-}90\%}$) obtained at CERN and ESRF for all samples at 77 K in self-field.

**Table 3: Summary of results from critical current measurements. *Corresponds to the strain at which the tape fractured.**

| Sample | $I_{c0}$ (A) | $\varepsilon_{95\%}$ (%) | $\varepsilon_{irr-5\%}$ (%) | $\varepsilon_{n\text{-}value\text{-}90\%}$ (%) |
|---|---|---|---|---|
| AMSC YBCO-1 | 112 | 0.42 | 1.07 | 1.06 |
| AMSC YBCO-2 | 109 | 0.42 | 1.03 | 0.96 |
| SuperPower YBCO-1 | 122 | 0.44 | 0.73 | 0.71 |
| SEI Bi-2223 Type HT-1 | 192 | 0.40* | n.m. | n.m. |
| SEI Bi-2223 Type HT-2 | 191 | 0.44* | n.m. | n.m. |
| SEI Bi-2223 Type HT-ESRF | 192 | 0.40 | n.m. | n.m. |
| SEI Bi-2223 Type G-1 | 220 | 0.17* | n.m. | n.m. |
| SEI Bi-2223 Type G-2 | 218 | 0.20* | n.m. | n.m. |
| OP processed Bi-2212-1 | 10.1 | 0.20 | 0.62 | 0.64 |
| OP processed Bi-2212-2 | 10.4 | 0.22 | 0.60 | 0.67 |
| OP processed Bi-2212-3 | 10.4 | 0.19 | n.m. | 0.64 |
| OP processed Bi-2212-ESRF | 10.6 | 0.16 | n.m. | 0.60 |

## 4.3 Combined X-ray diffraction, critical current, stress and strain measurements at ESRF

This section presents the results of the XRD experiments conducted at the ID15B beamline of ESRF. Combined lattice parameter, stress and strain measurements on one sample of OP processed Bi-2212 wire by OST was conducted at RT. Combined lattice parameter, critical current, stress and strain measurements were performed at 77 K on one sample of the same wire and a Bi-2223 Type HT tape by SEI.

**OP processed Bi-2212 wire**

The diffraction pattern of the OP processed Bi-2212 wire is shown in Figure 35 where the recorded intensity is plotted as a function of *d-spacing*. The segmented diffraction image is radially integrated and the intensities are summed in order to measure lattice parameters from the crystalline planes oriented both perpendicular and parallel to the applied load. The Bi-2212 peaks are identified by comparison with reference diffractograms [**Source**]

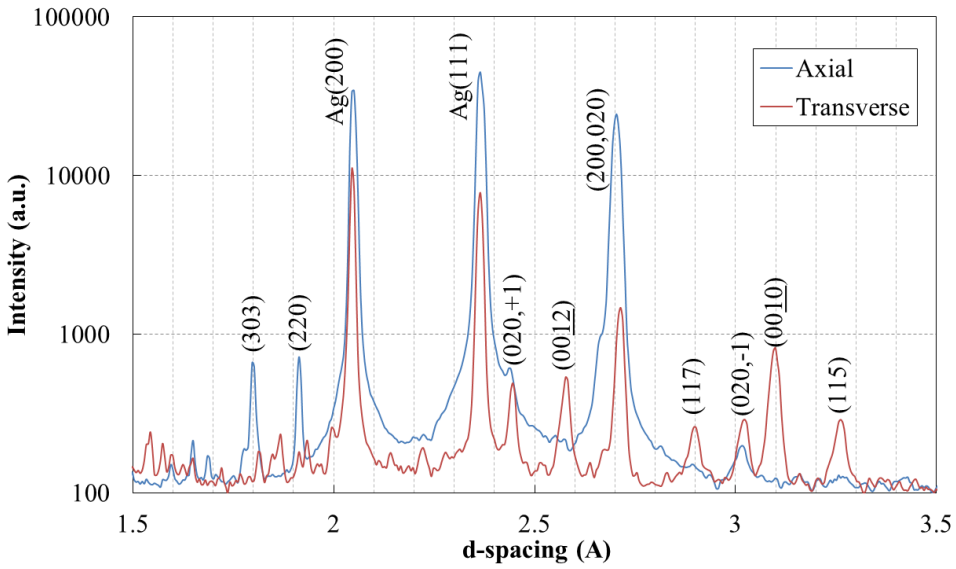


**Figure 35: Diffraction pattern of the OP processed Bi-2212 wire at 0% strain at RT. Annotations labels the Miller indexes of the Bi-2212 peaks, and two silver peaks.**

In Figure 36 the average axial and transverse elastic Bi-2212 strain is plotted as a function of wire strain measured by the extensometer at RT. The relative change in *d-spacing* is determined by normalizing the measured *d-spacing* to that at 0% extensometer strain. The engineering stress-strain curve acquired simultaneously is also shown for comparison. The graph shows a near linear/elastic increase in relative *d-spacing* until a plateau is reached, suggesting filament relaxation, at the same point as the stress plateaus. Bi-2212 peaks fitted had Miller indexes in axial direction: (200), (303) and (400), and in transversal direction: (00$\underline{1}$2), (00$\underline{1}$0), (008), (020) and (020,$\pm$1).

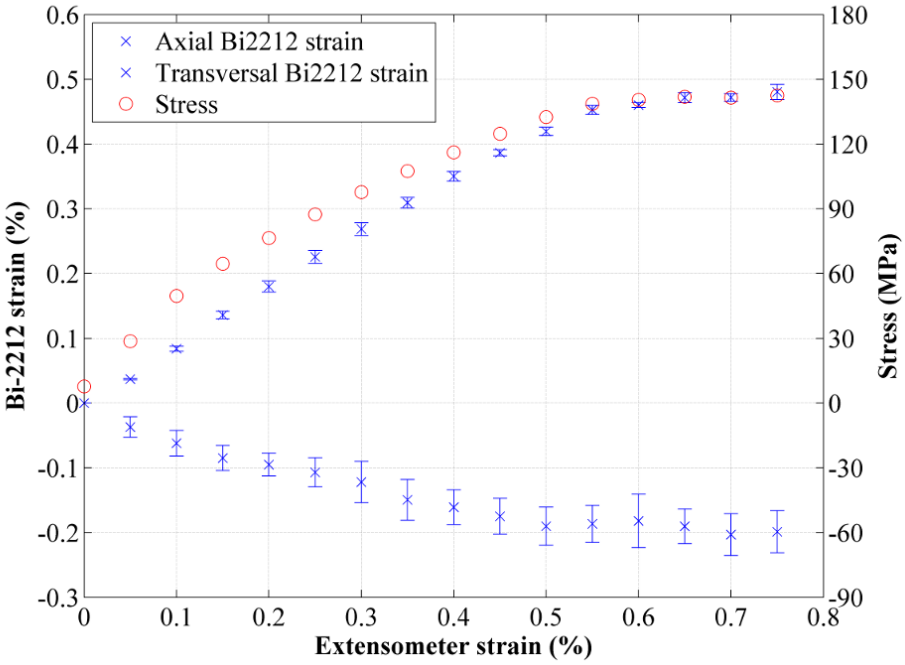


**Figure 36: Elastic strain calculated from the relative Bi-2212 *d-spacing* changes with respect to the *d-spacing* at zero strain in axial and transverse direction as a function of the wire strain at RT. The strain values are the average for all reflections in a given direction, and the error bars show the scatter of the results. The engineering stress-strain curve is shown for comparison.**

Figure 37 shows the relative change in *d-spacing* of a (200) peak at 77 K as a function of extensometer strain, compared with the simultaneously acquired curves for $I_c/I_{c0}$, *n-value* and $\sigma(\varepsilon)$. The relative change in *d-spacing* shows elastic behavior up to the $\varepsilon_{irr-5\%}$ where $I_c$ and *n-value* drops drastically and the engineering stress-strain curve plateaus. This can be explained by filament fractures as they relax during loading.

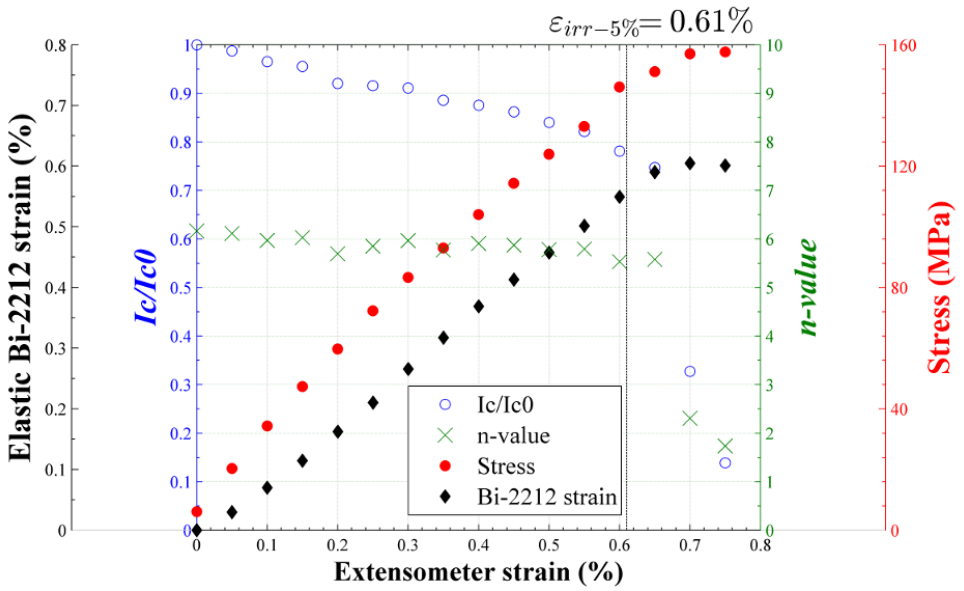


**Figure 37: Comparison of Bi-2212 wire relative $I_c$, *n-value*, stress and axial Bi-2212 strain variations as a function of the composite wire strain all measured simultaneously at 77 K.**

### Bi-2223 Type HT tape by SEI

Due to an error in the experiment a diffraction image, stress and $I_c$ was not obtained at 0.05% strain. The sample fractured outside of the extensometer gage length and beamline while increasing the strain from 0.46%, following the plateau of the elastic Bi-2223 strain curve.

Figure 38 shows the axial and transverse Bi-2223 (200) *d-spacing* changes as a function of wire strain. Assuming that a nearly stress free Bi-2223 lattice parameter is measured when the axial and the transverse lattice parameters intersects, it can be seen that the Bi-2223 filaments are initially under an axial pre-compression of about 0.08%.

In Figure 39 the $I_c/I_{c0}$, elastic Bi-2223 strain, *n-value*, and wire stress are plotted as a function of applied wire strain. Filament relaxation is observed at around 0.4% strain indicating filament damage, and complete filament rupture is observed at 0.46%, where a sharp drop in $I_c$ and *n-value* is observed, just before total sample fracture.

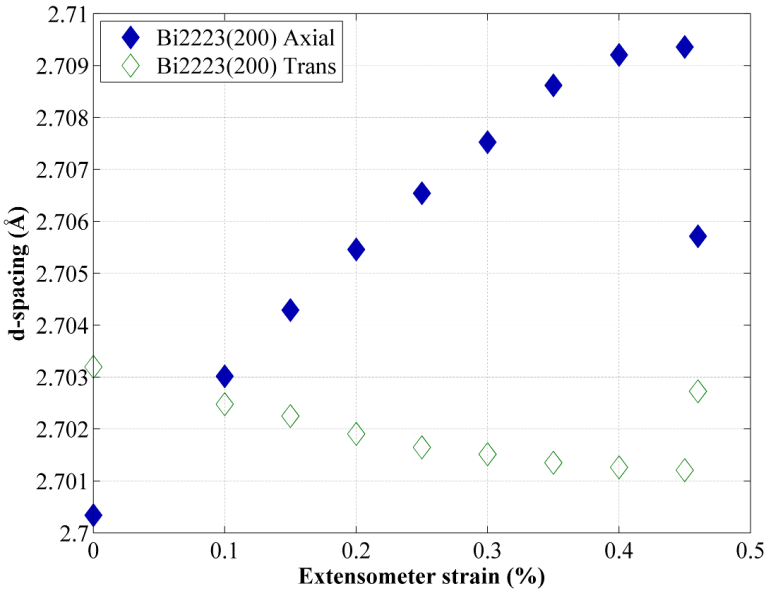


**Figure 38: Axial and transverse Bi-2223 (200) *d-spacing* as a function of extensometer strain at 77 K suggesting pre-compression.**

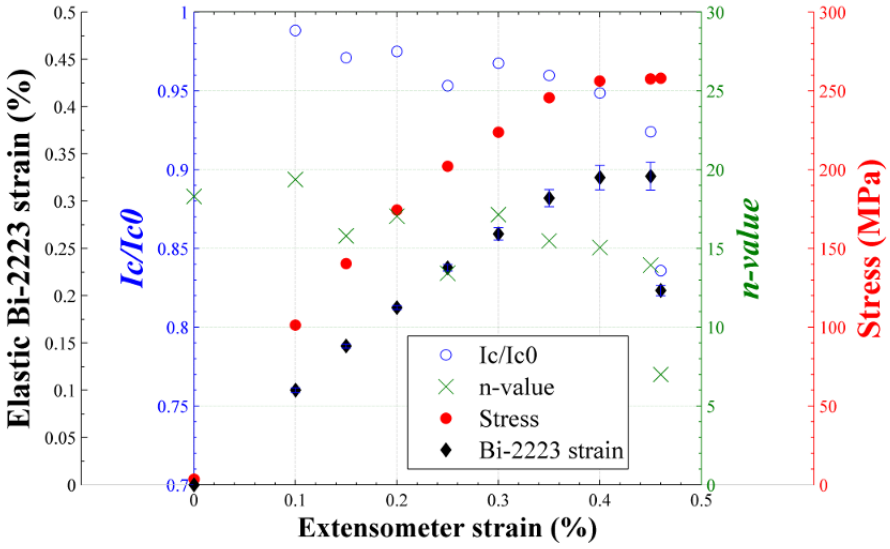


**Figure 39: Comparison of Bi-2223 tape relative $I_c$, *n-value*, stress and axial Bi-2223 strain variations as a function of the composite wire strain all measured simultaneously at 77 K.**

# 5 Discussion

In this thesis the results of the characterization of five different HTS, notably two YBCO monofilament tapes, two Bi-2223 multifilament tapes and one Bi-2212 multifilament wire are presented. For the characterizations a universal test machine could be used that had been equipped by the manufacturer with a lifting platform and a cryostat integrated into a reverse frame to allow stress-strain experiments in liquid nitrogen.

An important part of this thesis was the careful calibration of the MTS clip-on extensometer using a calibration set-up provided by KEK (see Figure 9). The MTS extensometer results were also compared to those obtained with another type of extensometer commonly used for the characterization of superconductors. This has guaranteed the accuracy and precision of the strain measurements that are reported in this thesis. The simultaneously measured d-spacing changes have given additional confidence in the accuracy of the extensometer strain measurements.

**Mechanical strength of the different HTS**
The comparison of the stress-strain curves presented in Figure 24 shows that the SuperPower YBCO tape has the highest mechanical strength of all HTS tested, exhibiting near linear elastic deformation up to a stress of 600 MPa. The high mechanical strength is mainly due to the strong Hastelloy C-276 substrate [23]. The AMSC YBCO tape with a Ni-5%at.W substrate has somewhat lower mechanical strength and its 0.2% offset yield strength is about 270 MPa lower than that of the tape produced by SuperPower.

The non-reinforced (type G) and reinforced (type HT) Bi-2223 tapes by SEI fractured when strained above 0.20% and 0.41%, respectively. Except one type HT tape that ruptured slightly above 0.46%, all Bi-2223 tapes fractured at the grips, probably due to stress concentrations in the tapes where they were fixed to the grips. The OP processed Bi-2212 wire can be strained more than the Bi-2223 tapes, but its tensile strength is with about 180 MPa relatively low.

**Strain dependent critical current measurements**
A specialized set of sample grips had to be utilized in order to perform strain dependent critical current measurements on HTS using the UTM. The design of the special grips that allow to connect the current leads and to electrically insulate the superconductor sample from the test equipment was supplied by KEK (see Figure 8 (a)). The plastic insulation of the sample has also served as mechanical protection, minimizing stress concentrations at the grips where the samples are fixed. The voltage taps with a distance of 20 mm could be

soldered inside the two knives of the extensometer, which has a gage length of 25 mm (see Figure 8 (b)). A low melting temperature solder was used for connection the voltage taps in order not to degrade the HTS samples. An existing Ic test set-up could be used for the measurements at CERN.

Typically $I_c(\varepsilon)$ measurements are performed by soldering the superconductor onto the sample holder of so-called Walters springs [24] and bending springs [25]. There are several advantages of the set-up presented in this thesis where a straight sample is free to contract during cooling down. Because the wire and tape samples are not bended there are no strain gradients across the sample cross sections. Strain and stress can be measured simultaneously with the critical current, and there is full control of the load during the entire experiment, including the cooling down from RT to 77 K, and there is no influence of the sample holder material on the sample stress state after cooling down. Only relatively short 150 mm-long samples are needed, as compared to the typically 1000 mm long samples needed for experiments with Walters springs. A main disadvantage of this set-up is that measurements in compression are not possible. Because of the relatively small test currents of up to 200 A, and due to the relatively small voltage tap distance of only 20 mm, $I_c$ measurements are less sensitive as those performed with a Walters spring.

**Comparison of the strain dependent $I_c$ degradation of the different HTS**

Figure 40 shows a comparison of the relative $I_c$ degradation of the five HTS studied. The $I_c$ is normalized to the sample's respective $I_{c0}$. It can be seen that the initial reversible Ic degradation characteristics of the YBCO and Bi-2223 tapes is quite comparable. The Bi-2212 wire shows a relatively stronger reversible degradation, which may be explained by the fact that the wire is at 77 K very close to its critical temperature.

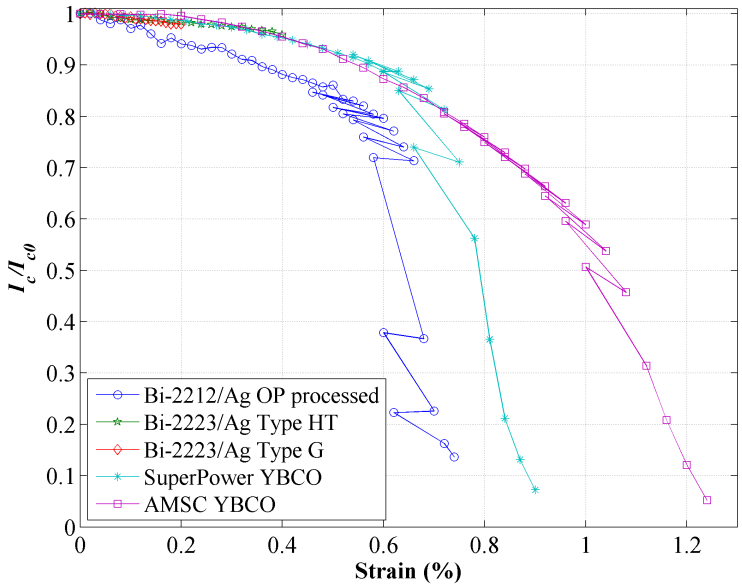


**Figure 40: Comparison of the critical current degradation as a function of tensile strain.**

The irreversible strain limit of the YBCO and Bi-2223 tapes and the Bi-2212 wire are heavily influenced by the mechanical properties of the substrate, reinforcement and matrix. The YBCO tape by AMSC can be strained by 1% before the irreversible strain limit is reached. This is the highest $\varepsilon_{irr-5\%}$ value observed in this work. The YBCO tape by SuperPower exhibits an irreversible strain limit of $\varepsilon_{irr-5\%} = 0.7\%$.

The irreversible strain limit of the OP processed Bi-2212 wire is 0.6%, which is slightly lower than that of the YBCO tape by SuperPower. However, the critical stress at the irreversible strain limit is approximately 150 MPa, thus about 4 times lower than that critical stress of the SuperPower tape. One Bi-2223 type HT tape could be strained slightly above 0.46%, and a drop in n-value was observed at 0.46%. This suggests that the irreversible strain limit is fairly close to 0.46%. Apart from this sample all other Bi-2223 tapes by SEI showed no irreversible degradation before they ruptured.

The *n-value* changes ares a good indication to detect the irreversible degradation of the filaments [26]. In the present work the $I_c$ measurements of YBCO tapes and Bi-2212 wires suggest good correlation between the irreversible strain limit $\varepsilon_{irr-5\%}$ and the strain which produces a 10% reduction in *n-value* (see Table 3).

**Integration of the UTM in the synchrotron beamline**
The test configuration using a free standing straight sample has allowed to perform for the first time measurements of lattice parameters by X-ray diffraction in a high energy synchrotron beamline simultaneously with the measurement of the critical current, extensometer strain and stress.

The main constraints for the integration of the UTM into the ID15B beamline of the European Synchrotron were the maximum weight of 100 kg that could be loaded onto the sample translation and rotation stages, the distance of 275±20 mm from the top of the sample stages to the sample center, and an X-ray transmission through the $LN_2$ filled cryostat of roughly 50% or better.

A lightweight connecting plate used to fix the UTM to the sample translation stage. Due to the limited height of the X-ray beam the reverse frame had to be lowered as far as possible. The X-ray transparent cryostat that was required for the experiments was made of sheets of stainless steel, encapsulated in Styrofoam. The cryostat had two windows of PET for the incident and diffracted beam.

A mobile critical current measurement system was required in order to perform experiments at the ID15B beamline at ESRF. The set-up consisted of a power supply and a multimeter that were controlled using a LabVIEW program, allowing for efficient acquisition of V-I curves from HTS with different critical currents.

**Combined lattice parameter, Ic, stress and strain measurements**
In the Bi-2212 wire and in the Bi-2223 tape the d-spacing changes of the superconducting phase could be measure in axial and in transverse direction. The results show that before application of an external load the Bi-2212 and the Bi-2223 filaments are in axial pre-compression, presumably due to the different thermal expansion coefficients of Bi-2212, Bi-2223 and Ag. The axial d-spacing of the filaments increases linearly with the extensometer wire strain, indicating a linear elastic behavior up to a strain of about 0.6% and 0.4% for the Bi-2212 and Bi-2223 filaments, respectively. Increasing the strain further does not change the axial lattice parameter, indicating that the filaments cannot carry higher loads anymore.

# 6 Conclusion

The main goal of this thesis work was to set up an experiment for the characterization of the electromechanical properties of HTS tapes and wires in liquid nitrogen in self-field.

In order to achieve this the following hardware modifications had to be made at an existing tensile test set-up:

- Adding the grips with current lead connectors to the UTM
- Instrument the samples with voltage taps and electrical insulation from the grips
- Design an X-ray transparent and demountable $LN_2$ cryostat
- Lowering the reverse load frame to be compatible with the X-ray beam position in the ID15B beam line
- Design a lightweight adapter for connecting the UTM with the sample stages of the ID15B beamline

Additionally, a new mobile critical current measurement set-up with a LabVIEW control and data acquisition program had to be developed for the experiment in the ID15B beamline. The successful integration of the set-up in the ID15B beamline has allowed for the first time to acquire simultaneously the diffraction pattern together with critical current, stress and strain measurements.

The following experimental procedures had to be established:

- 77 K calibration of the extensometer
- Acquisition of stress-strain curves in $LN_2$
- Acquisition of critical current measurements as a function of the superconductor strain in $LN_2$ at self-field
- Simultaneous acquisition of diffraction pattern with critical current, stress and strain measurements in the ID15B beamline

Throughout this thesis work a large amount of experimental data has been acquired and needed to be analyzed efficiently using various programs. The stress-strain and critical current measurement data was analyzed using Excel. Segmentation and radial integration of diffraction pattern was done using the FIT2D software. Over 1000 diffraction peaks were fitted with a newly developed MatLab script.

The electromechanical properties of five different HTS have been thoroughly characterized. The results of the Bi-2212 wire have been submitted as a scientific article [27].

The present set-up has great potential to measure the strain dependency of the critical current in superconductors which a lower critical temperature than 77 K, such as $MgB_2$ and $Nb_3Sn$, if equipped with a cryocooler. In future experiments with similar procedures including XRD and HTS, a stress-free powder of the superconducting elements should be used at RT and 77 K in order to determine pre-stresses in the wire.

# References

[1] M. Brice, "Cross section of an lhc dipole in the tunnel." Jul 2011, obtained: 06.10.2014 from https://cds.cern.ch/record/1365795?ln=en.

[2] O. S. Bruening, P. Collier, P. Lebrun, S. Myers, R. Ostojic, J. Poole, and P. Proudlock, *LHC Design Report*. Geneva: CERN, 2004.

[3] L. Rossi, "Superconductivity: its role, its success and its setbacks in the large hadron collider of cern," *Superconductor Science and Technology*, vol. 23, no. 3, p. 034001, 2010, DOI: http://stacks.iop.org/0953-2048/23/i=3/a=034001.

[4] W. D. Markiewicz, D. C. Larbalestier, H. W. Weijers, A. J. Voran, K. W. Pickard, W. R. Sheppard, J. Jaroszynski, A. Xu, R. Walsh, J. Lu, A. Gavrilin, and P. Noyes, "Design of a superconducting 32 t magnet with rebco high field coils," *IEEE Transactions on Applied Superconductivity*, vol. 22, no. 3, 2012, DOI: http://dx.doi.org/10.1109/TASC.2011.2174952.

[5] J. Schwartz, T. Effio, X. Liu, Q. Le, A. Mbaruku, H. Schneider-Muntau, T. Shen, H. Song, U. Trociewitz, X. Wang, and H. Weijers, "High field superconducting solenoids via high temperature superconductors," *IEEE Transactions on Applied Superconductivity*, vol. 18, no. 2, pp. 70–81, 2008, DOI: http://dx.doi.org/10.1109/TASC.2008.921363.

[6] R. P. Walsh, D. McRae, W. D. Markiewicz, J. Lu, and V. J. Toplosky, "The 77-k stress and strain dependence of the critical current of ybco coated conductors and lap joints," *IEEE Transactions on Applied Superconductivity*, vol. 22, no. 1, 2012, DOI: http://dx.doi.org/10.1109/TASC.2011.2182349.

[7] K. Katagiri, Y. Tsunematsu, Y. Ishikawa, T. Takahashi, K. Kasaba, T. Kuroda, and K. Itoh, "Strain characteristics of critical current in rabits/y-ba-cu-o coated conductors," *Physica C: Superconductivity*, vol. 468, no. 15–20, pp. p. 1697 – 1701, 2008, proceedings of the 20th International Symposium on Superconductivity (ISS 2007). DOI: http://dx.doi.org/10.1016/j.physc.2008.05.244.

[8] G. E. Dieter, *Materials Science and Engineering Series: Mechanical Metallurgy*. United States of America, USA: McGraw-Hill, Inc., 1976.

[9] F. S. Smith and J. Hashemi, *Foundations of materials science and engineering*. New York: McGraw-Hill Companies, Inc., 2011.

[10] J. Ekin, *Experimental techniques for low-temperature measurements*. New York: Oxford University Press, 2006.

[11] T. Sheahen, *Introduction to High-Temperature Superconductivity.* New York, NY: Plenum press, 1994.

[12] W. H. Bragg and W. L. Bragg, "The reflection of x-rays by crystals," *Proceedings of the Royal Society of London A: Mathematical, Physical and Engineering Sciences*, vol. 88, no. 605, pp. 428–438, 1913, DOI: http://dx.doi.org/10.1098/rspa.1913.0040.

[13] P. Yanisko and D. Croll, "Use nitrogen safely," (2012), [Online]. Cited: 15.10.2014 from http://www.airproducts.com/~/media/downloads/article/U/en-use-nitrogen-safely-312-12-023.pdf.

[14] AMSC (2014), "Amperium® brass laminated wire type 8700," [Online]. Cited: 02.06.2014 from http://www.amsc.com/documents/brass-laminated-amperium153-wire-data-sheet.

[15] M. Putti, E. Bellingeri, C. Ferdeghini, G. Grasso, S. Roncallo, D. Mazzone, G. Zanicchi, and M. O. Rikel, "The thermal conductivity of silver and silver alloy sheaths for bi-2223 tapes," *Physica C: Superconductivity*, vol. 372–376, Part 3, no. 0, pp. 1835 – 1838, 2002, DOI: http://dx.doi.org/10.1016/S0921-4534(02)01003-1.

[16] Angewandte System Technink (AST) (2013), "Kap-s, kap-e force transducer," [Online]. Cited: 30.04.2014 from http://www.ast.de/files/pdf/mess-und-regeltechnik/sensoren/E_KMT_KAP-S.pdf.

[17] MTS Systems Corporation (2014), "Services and accessories," [Online]. Cited: 02.04.2014 from https://www.mts.com/ucm/groups/public/documents/library/dev_003828.pdf.

[18] Lambda (2011), "Genesystm," [Online]. Cited: 04.02.2014 from http://www.us.tdk-lambda.com/hp/pdfs/data%20sheets/93507510.pdf.

[19] G. Willering, "New test station for hts superconductors cooled by ln2 in the hts-lab (b288)," *CERN-TE-MCS-SCD*, 2011.

[20] C. Scheuerlein, M. D. Michiel, F. Buta, B. Seeber, C. Senatore, R. Flükiger, T. Siegrist, T. Besara, J. Kadar, B. Bordini, A. Ballarino, and L. Bottura, "Stress distribution and lattice distortions in nb 3 sn multifilament wires under uniaxial tensile loading at 4.2 k," *Superconductor Science and Technology*, vol. 27, no. 4, p. 044021, 2014, DOI: http://stacks.iop.org/0953-2048/27/i=4/a=044021.

[21] H. D. G. C. K. (2006), "User's manual xy-stages series 5102," http://www.xhuber.de/fileadmin/user_upload/downloads/usermanuals/series_5102_en.pdf.

[22] A. Hammersley, "The fit2d home page," http://www.esrf.eu/computing/scientific/FIT2D/.

[23] C. Clickner, J. Ekin, N. Cheggour, C. Thieme, Y. Qiao, Y. Xie, and A. Goyal, "Mechanical properties of pure ni and ni-alloy substrate materials for y–ba–cu–o coated superconductors," *Cryogenics*, vol. 46, no. 6, pp. 432 – 438, 2006, DOI: http://dx.doi.org/10.1016/j.cryogenics.2006.01.014.

[24] C. Walters, I. Davidson, and G. Tuck, "Long sample high sensitivity critical current measurements under strain," *Cryogenics*, vol. 26, no. 7, pp. 406–412, 1986, DOI: http://dx.doi.org/10.1016/0011-2275(86)90085-8.

[25] B. Ten Haken, H. ten Kate, and J. Tenbrink, "Compressive and tensile axial strain reduced critical currents in bi-2212 conductors," *IEEE Transactions on Applied Superconductivity*, vol. 5, no. 2, pp. 1298–1301, June 1995, DOI: http://dx.doi.org/10.1109/77.402800.

[26] L. Goodrich, N. Cheggour, X. Lu, J. Splett, T. Stauffer, and B. Filla, "Method for determining the irreversible strain limit of nb 3 sn wires," *Superconductor Science and Technology*, vol. 24, no. 7, p. 075022, 2011, DOI: http://dx.doi.org/10.1088/0953-2048/24/7/075022.

[27] R. Bjoerstad, C. Scheuerlein, M. Rikel, A. Ballarino, L. Bottura, J. Jiang, M. Matras, M. Sugano, and J. Hudspeth, "Strain induced irrveversible critical current degradation in highly dense bi-2212 round wire," *Superconducting Science and Technology*, submitted.

# A Glossary

## Unit abbreviation

| | |
|---|---|
| **A** | ampere |
| °C | degrees Celsius |
| **K** | degrees Kelvin |
| **mm** | millimeter |
| $\mu$**V/cm** | electrical field strength |
| **MPa** | megapascal |
| **s** | second |
| **V** | voltage |

## Acronyms and Abbreviations

| | |
|---|---|
| **Ag** | Atomic symbol of silver |
| **AMSC** | American superconductors |
| **BSCCO** | Bismuth-Strontium-Calcium-Copper-Oxide based superconductor |
| **CERN** | European Organization for Nuclear Research |
| **CF** | Calibration factor, used to determine true displacement of extensometer |
| **H&P** | Hegewald and Peschke |
| **HTS** | High-temperature superconductor, defined as materials which portrays superconducting properties at 77 K |
| **LHe** | Liquid helium |
| **LHC** | Large Hadron Collider |
| **$LN_2$** | Liquid nitrogen |
| **n.m.** | Not measured |
| **NbTi** | Niobium-titanium, superconducting material |
| **OP** | Overpressure, production phase of the Bi-2212 wires where the heat treatment is conducted in an atmosphere of 100 bars. |
| **UTM** | Universal test machine |
| **RT** | Room temperature, the ambient temperature in the experimental location |
| **SC** | Superconducting |
| **SEI** | Sumitomo electric industries |
| **YBCO** | Yttrium-Barium-Copper-Oxide based superconductor |
| **XRD** | X-ray diffraction |

## Variables

| | |
|---|---|
| $A_0$ | Original unloaded cross-sectional area of a sample. Unit: $mm^2$ |
| $E_a$ | Unloading modulus of elasticity. Unit: $GPa$ |
| $E$ | Electrical field strength. Unit: $\mu V/cm$ |
| $\varepsilon_{95\%}$ | Strain at 95% retention of critical current. Unit: % |
| $\varepsilon_{max}$ | Strain at fracture. Unit: % |
| $\varepsilon_{p0.2}$ | 0.2% offset yield strain, determined from $E_a$. Unit: % |
| $\varepsilon_{p0.02}$ | 0.02% offset yield strain, determined from $E_a$. Unit: % |
| $\varepsilon_{irr-5\%}$ | Irreversible strain limit, defined as the strain where the reversible strain effect dissipates. Unit: % |
| $I_c$ | Critical current of a superconductor. Unit: $GPa$ |
| $I_{c0}$ | Critical current of an unloaded superconductor. Unit: $A$ |
| $R_{max}$ | Stress at fracture. Unit: $MPa$ |
| $R_{p0.2}$ | 0.2% offset yield strength, determined from $E_a$. Unit: $MPa$ |
| $R_{p0.02}$ | 0.02% offset yield strength, determined from $E_a$. Unit: $MPa$ |
| $I_c / I_{c0}$ | Relative critical current degradation. Unit: $-$ |
| $I$ | Current. Unit: $A$ |

# B Engineering stress-strain curves

This section presents the engineering stress-strain curves acquired at 77 K used to characterize the mechanical properties of samples.

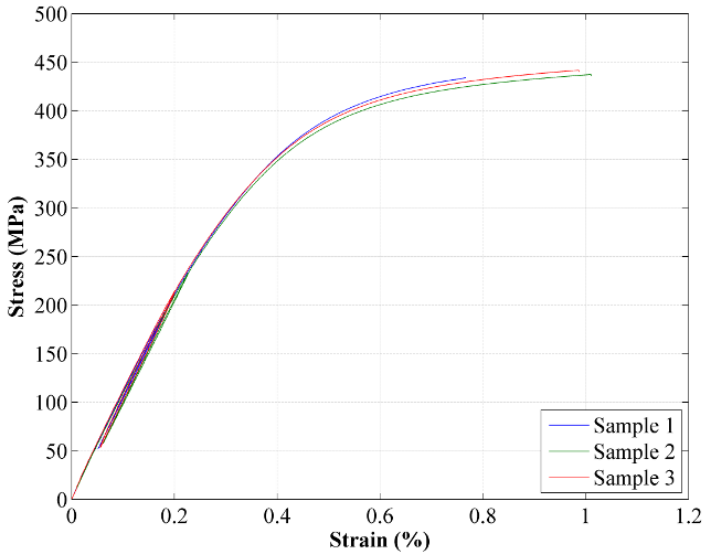


**Engineering stress-strain curve of three samples of YBCO tapes by AMSC**

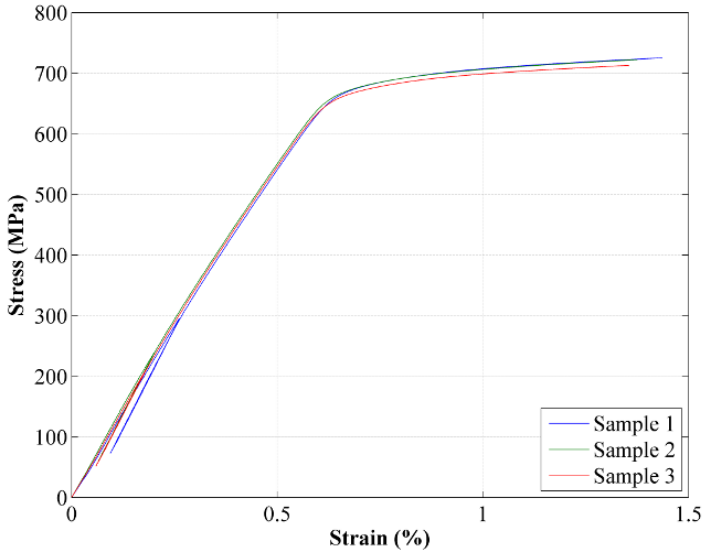


**Engineering stress-strain curve of three samples of YBCO tapes by SuperPower**

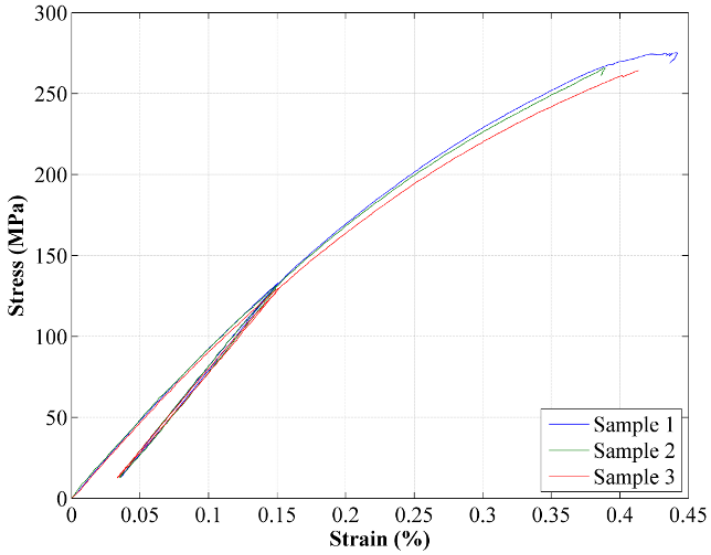


**Engineering stress-strain curve of three samples of Bi-2223 Type HT tapes by SEI**

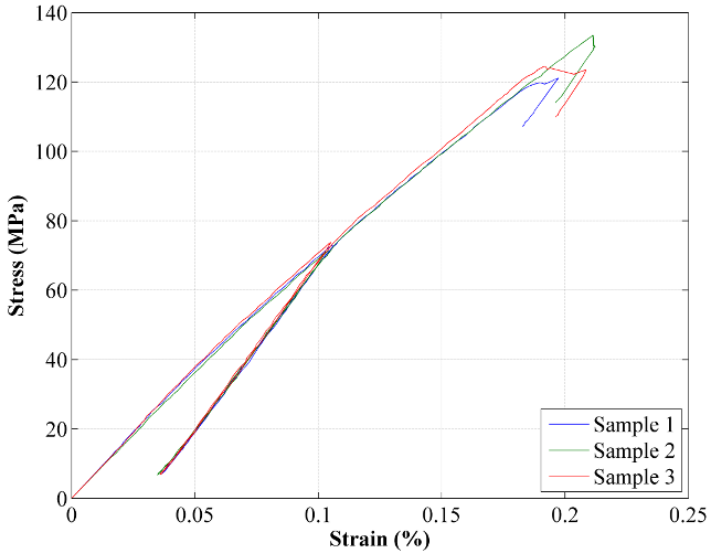


**Engineering stress-strain curve of three samples of Bi-2223 Type G tapes by SEI**

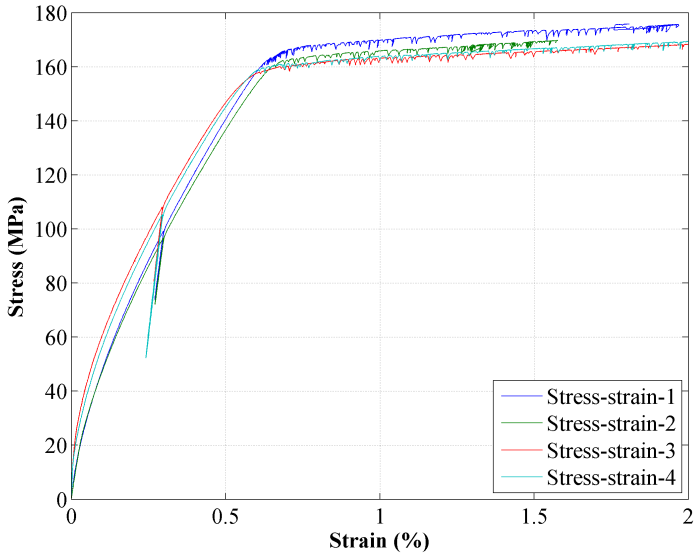


**Engineering stress-strain curve of four samples of OP processed Bi-2212 wires by OST**

# C Technical drawings

This section includes the technical drawings made for the connecting plate and the cryostat used in the experiments at ESRF.

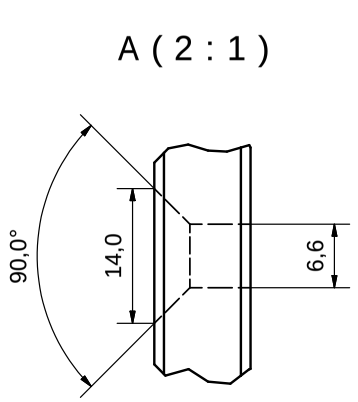


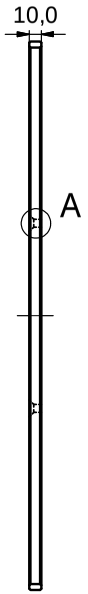


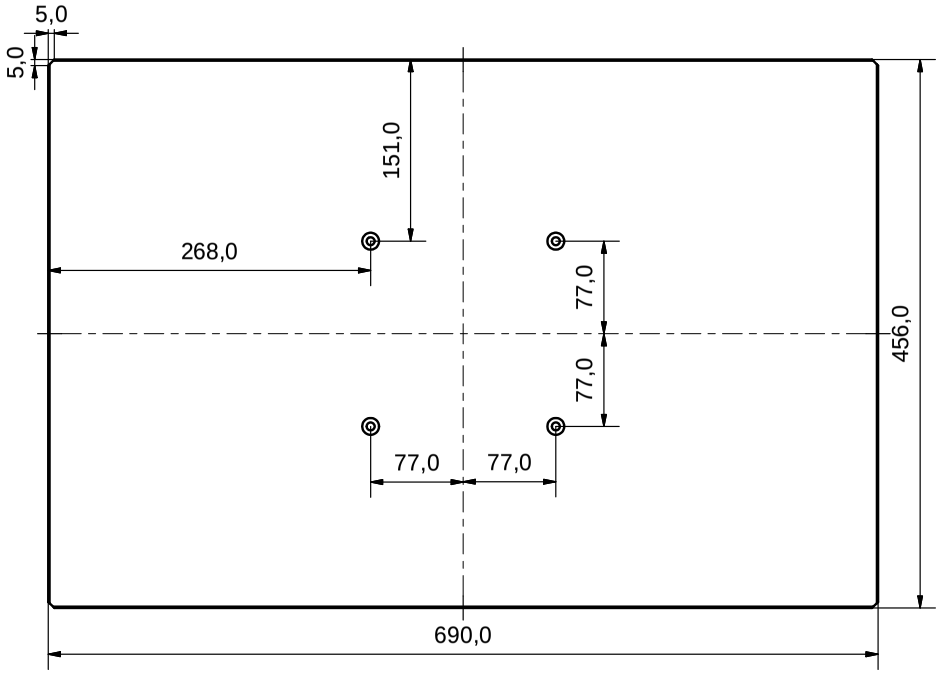


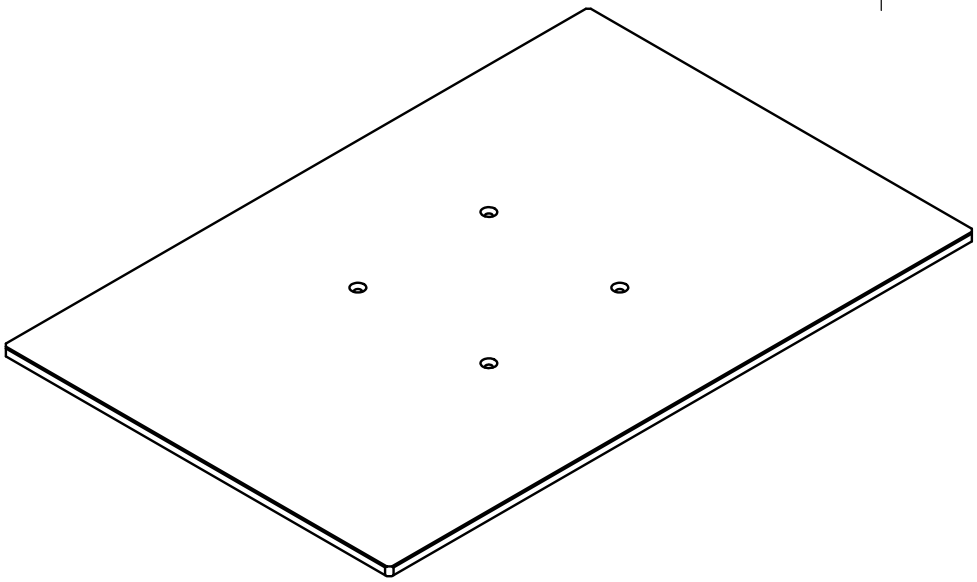

| | | | | | |
|---|---|---|---|---|---|
| All edges: 1 mm chamfer | | | | | |
| Material: Aluminium | | | | | |
| Estimated volume: 3146.4 cm^3 | | | | | |
| Estimated weight: 8.53 kg (density: 2.71 g/cm^3) | | | | | |
| Designed by: rbjoerst | Checked by: | Approved by: | Date: | Date: 16/10/2014 | |
| | | Connecting plate | | Edition: | Sheet: 1 / 1 |

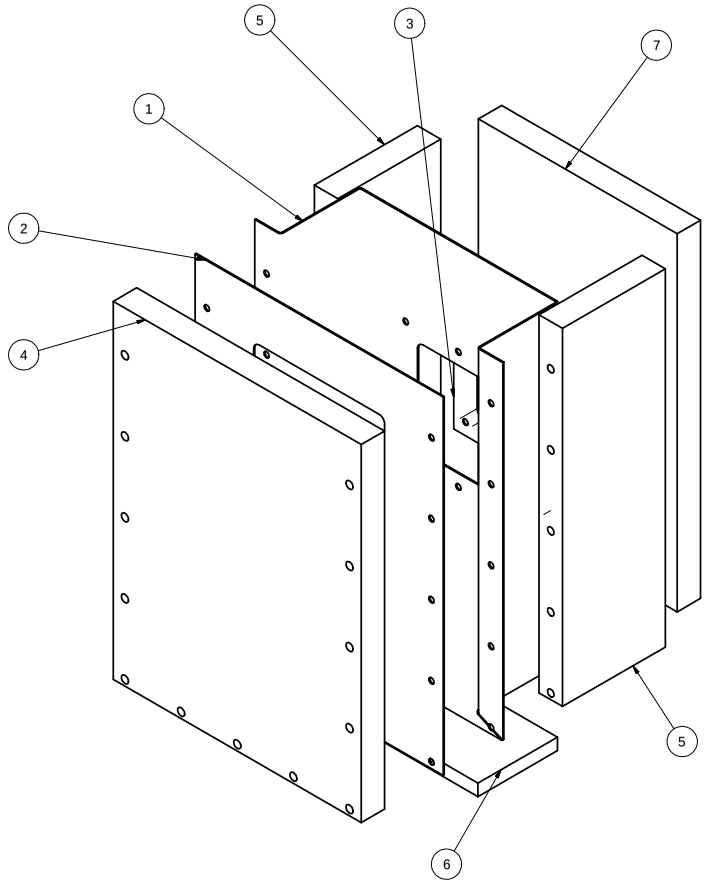


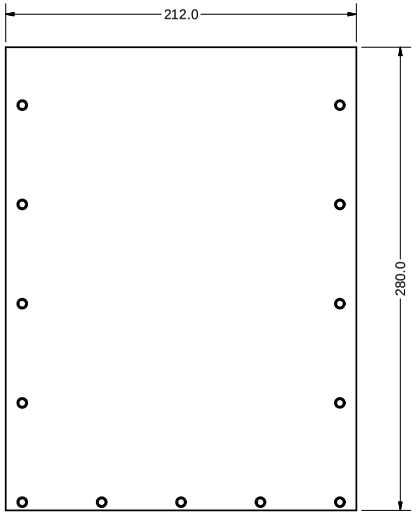


| PARTS LIST | | | |
|---|---|---|---|
| ITEM | QTY | PART NUMBER | DESCRIPTION |
| 1 | 1 | Cryostat frame | |
| 2 | 1 | Windowed lid | |
| 3 | 1 | Rear window frame | |
| 4 | 1 | Styrofoam front | |
| 5 | 2 | Styrofoam side | |
| 6 | 1 | Styrofoam bottom | |
| 7 | 1 | Styrofoam back | |

| | | |
|---|---|---|
| DRAWN Roger Bjoerstad | 19/01/2015 | CERN |
| CHECKED | | TITLE: Cryostat assembly |
| QA | | |
| MFG | | |
| APPROVED | | |
| | | SIZE C / DWG NO Cryostat / REV |
| | | SCALE / SHEET 1 OF 8 |

Assembly is made with M4x10mm bolts and M4 nuts

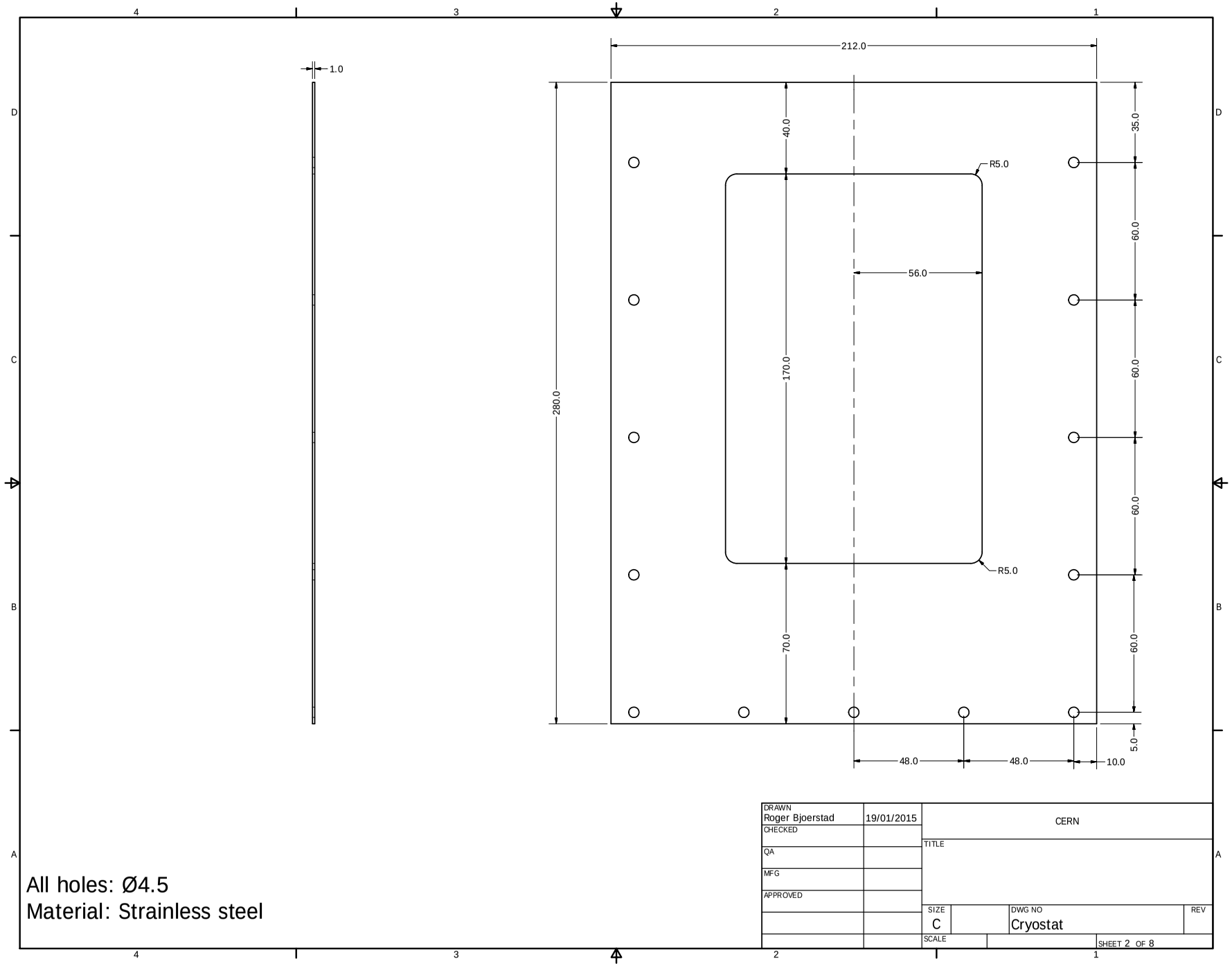


All holes: Ø4.5
Material: Strainless steel

| | | |
|---|---|---|
| DRAWN Roger Bjoerstad | 19/01/2015 | CERN |
| CHECKED | | TITLE |
| QA | | |
| MFG | | |
| APPROVED | | |
| | | SIZE C / DWG NO Cryostat / REV |
| | | SCALE / SHEET 2 OF 8 |

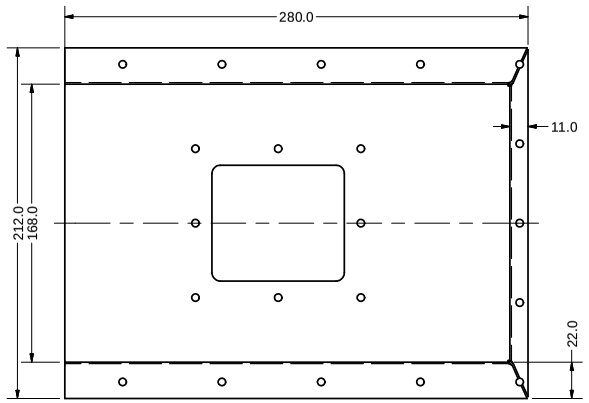



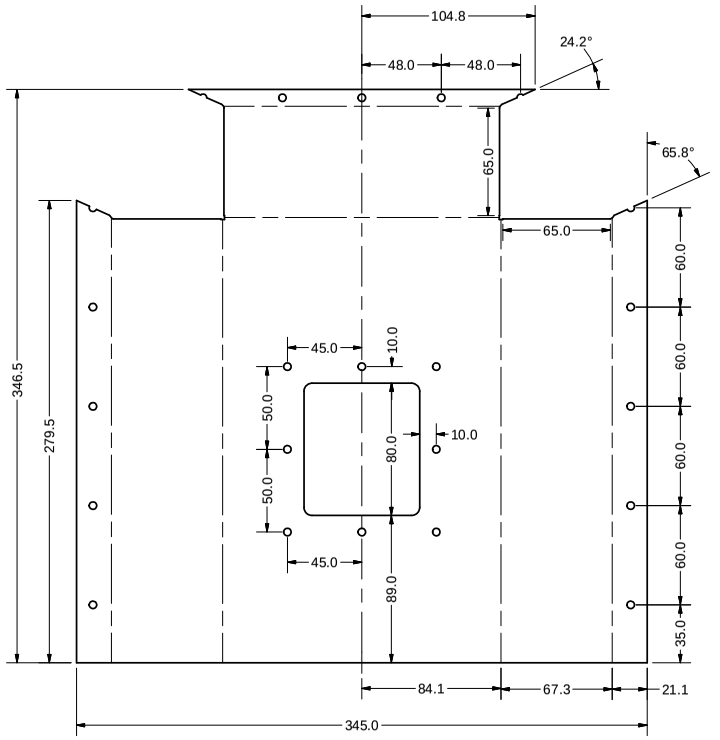


All holes: Ø4.5
Material: 1 mm Strainless steel sheet
Bend radius: 1 mm
Joins are closely welded

| | | |
|---|---|---|
| DRAWN Roger Bjoerstad | 19/01/2015 | CERN |
| CHECKED | | TITLE Cryostat frame |
| QA | | |
| MFG | | |
| APPROVED | | |
| | | SIZE C / DWG NO Cryostat / REV |
| | | SCALE / SHEET 3 OF 8 |

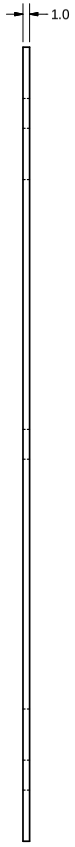


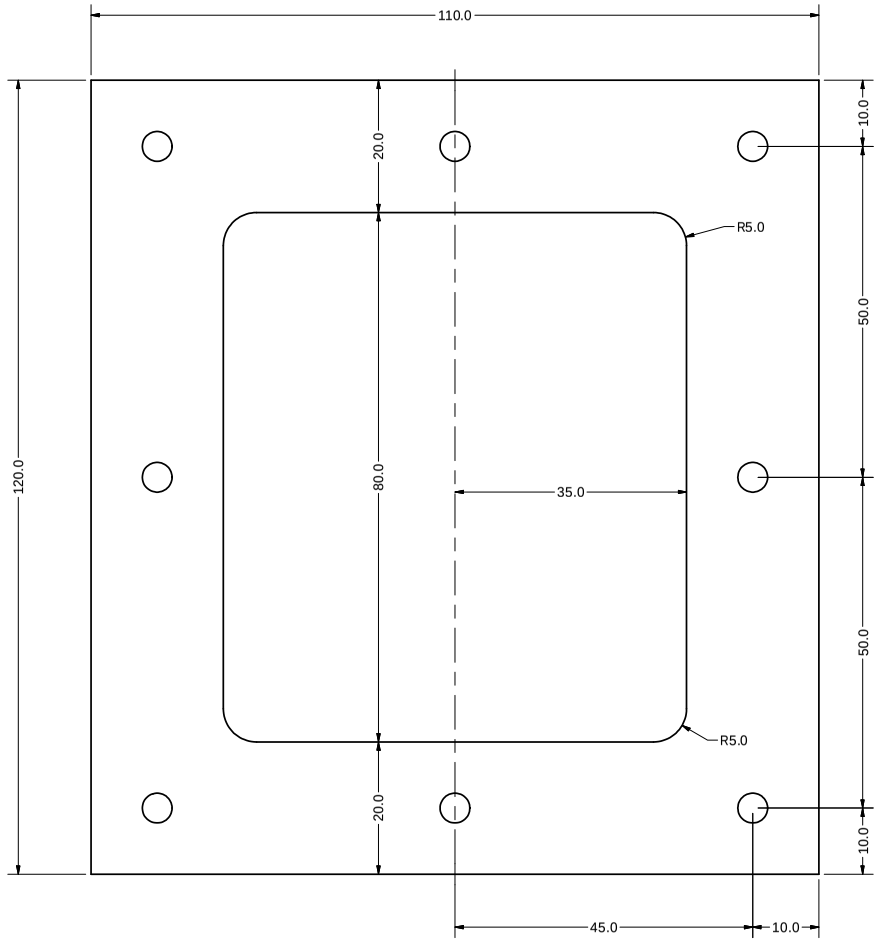


All holes: Ø4.5
Material: Strainless steel

| | | | |
|---|---|---|---|
| DRAWN Roger Bjoerstad | 19/01/2015 | CERN | |
| CHECKED | | TITLE Rear window lid | |
| QA | | | |
| MFG | | | |
| APPROVED | | | |
| | | SIZE C | DWG NO Cryostat |
| | | SCALE | SHEET 4 OF 8 |

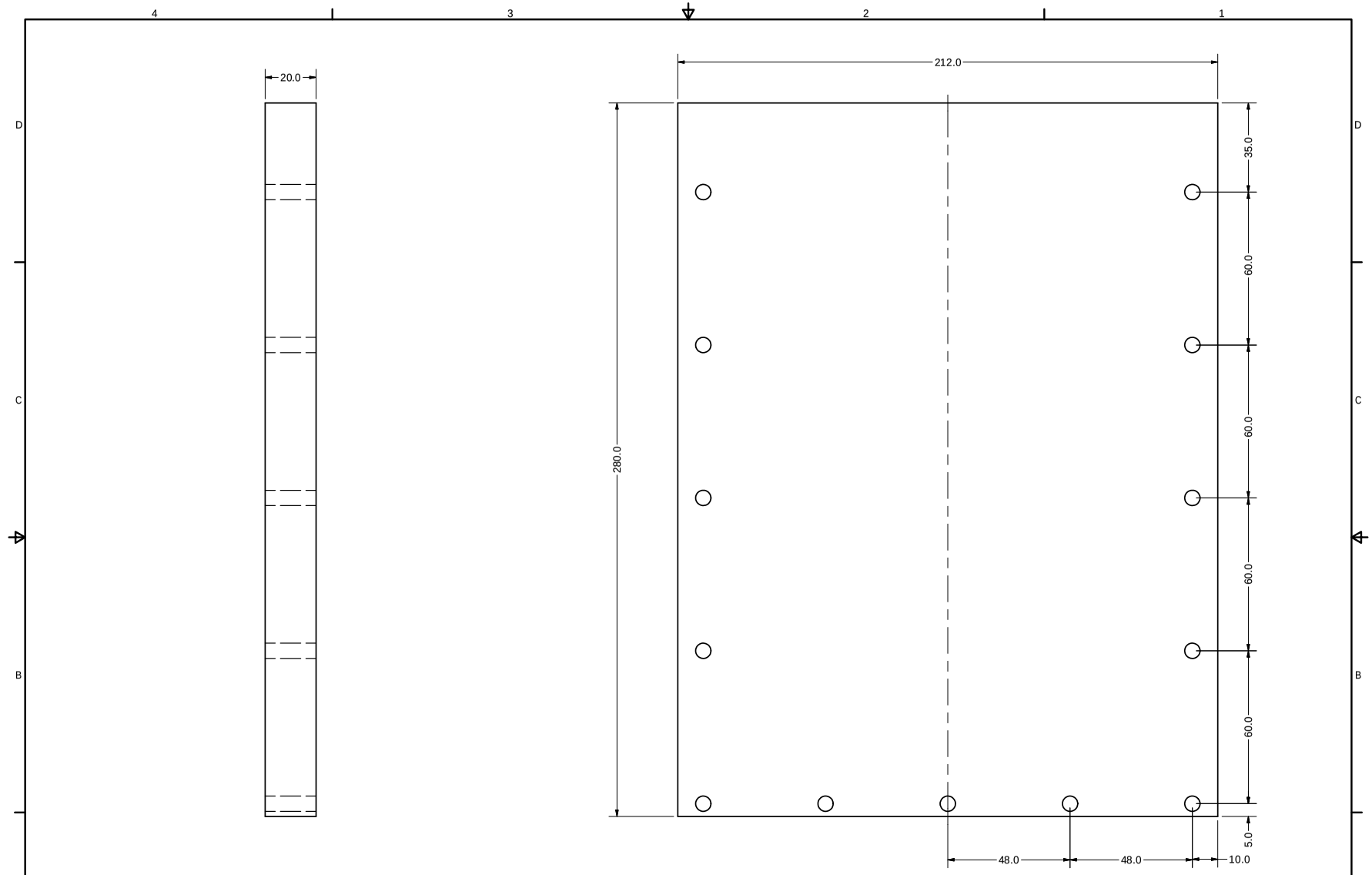


All holes: Ø6.0
Material: Styrofoam

| | | |
|---|---|---|
| DRAWN Roger Bjoerstad | 19/01/2015 | CERN |
| CHECKED | | TITLE: Styrofoam front |
| QA | | |
| MFG | | |
| APPROVED | | |
| | | SIZE C / DWG NO Cryostat / REV |
| | | SCALE / SHEET 5 OF 8 |

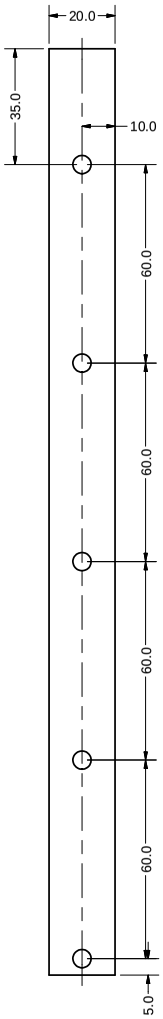


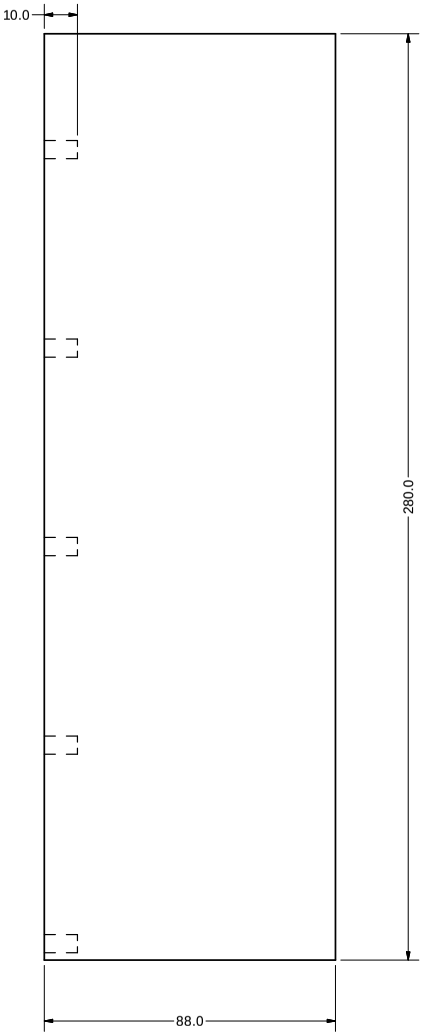


All holes: Ø5.5
Material: Styrofoam

| | | |
|---|---|---|
| DRAWN Roger Bjoerstad | 19/01/2015 | CERN |
| CHECKED | | TITLE: Styrofoam side |
| QA | | |
| MFG | | |
| APPROVED | | |
| | | SIZE C / DWG NO Cryostat / REV |
| | | SCALE / SHEET 6 OF 8 |

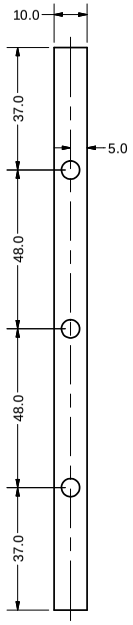


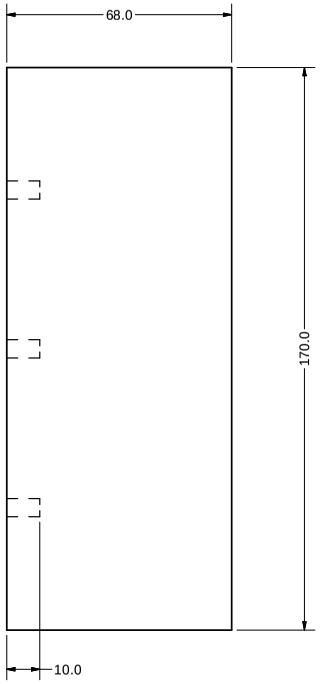


All holes: Ø5.5
Material: Styrofoam

| | | |
|---|---|---|
| DRAWN Roger Bjoerstad | 19/01/2015 | CERN |
| CHECKED | | TITLE: Styrofoam bottom |
| QA | | |
| MFG | | |
| APPROVED | | SIZE C \| DWG NO Cryostat \| REV |
| | | SCALE \| SHEET 7 OF 8 |

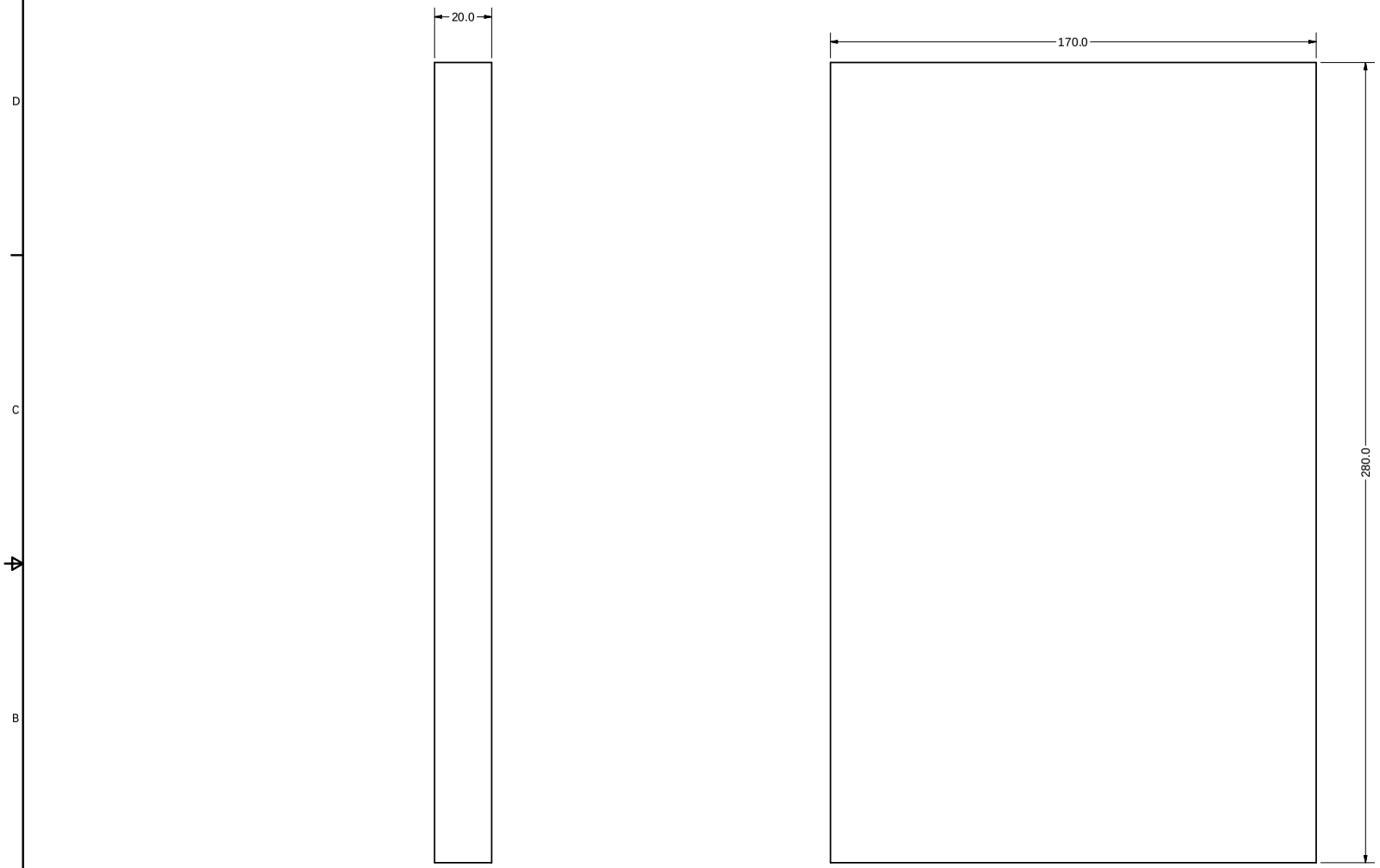


Material: Styrofoam

| | | |
|---|---|---|
| DRAWN Roger Bjoerstad | 19/01/2015 | CERN |
| CHECKED | | TITLE: Styrofoam back |
| QA | | |
| MFG | | |
| APPROVED | | |
| | | SIZE C \| DWG NO Cryostat \| REV |
| | | SCALE \| SHEET 8 OF 8 |